Multiple Model Spline Probability Hypothesis Density Filter

Rajiv Sithiravel, Mike McDonald, Bhashyam Balaji and Thiagalingam Kirubarajan

Abstract

The Probability Hypothesis Density (PHD) filter is an efficient algorithm for multitarget tracking in the presence of nonlinearities and/or non-Gaussian noise. The Sequential Monte Carlo (SMC) and Gaussian Mixture (GM) techniques are commonly used to implement the PHD filter. Recently, a new implementation of the PHD filter using B-splines with the capability to model any arbitrary density functions using only a few knots was proposed. The Spline PHD (SPHD) filter was found to be more robust than the SMC-PHD filter since it does not suffer from degeneracy and it was better than the GM-PHD implementation in terms of estimation accuracy, albeit with a higher computational complexity. In this paper, we propose a Multiple Model (MM) extension to the SPHD filter to track multiple maneuvering targets. Simulation results are presented to demonstrate the effectiveness of the new filter.

Index Terms

Maneuvering target tracking, Nonlinear filtering, Probability Hypothesis Density filter, Spline filter, Spline Probability Hypothesis Density filter.

I. Introduction

The Spline Probability Hypothesis Density (SPHD) filter [24] is the latest implementation of the Probability Hypothesis Density (PHD) filter. Just like the standard PHD filter, the SPHD filter avoids data association between measurements and tracks based on the Random Finite Set (RFS) methodology [13, 14, 15]. Since there is no explicit ordering in states or measurement sets, one can apply the finite set properties. The RFS formulation takes advantage of finite set properties and permits a Bayesian filtering framework to estimate the number of targets and the target states [14, 30] in the presence of clutter, false alarms and missed detections. For non-maneuvering multitarget tracking problems, the SPHD filter [24] can be an effective alternative to the Sequential Monte Carlo Probability Hypothesis Density (SMC-PHD) [20, 31], Gaussian Mixture Probability Hypothesis Density (GM-PHD) [32], Gaussian Mixture Particle Probability Hypothesis Density (GMP-PHD) [5,34], Gaussian Mixture Unscented Sequential Monte Carlo Probability Hypothesis Density (GM-USMC-PHD) [35], Gaussian Mixture Sequential Monte Carlo Probability Hypothesis Density (GM-SMC-PHD) [21], and the Auxiliary Particle Probability Hypothesis Density (AP-PHD) [3, 33] filters. The SPHD filter offers continuous estimates of the probability hypothesis density of the multitarget state for any

R.Sithiravel, M.McDonald and B.Balaji are with the Radar System Section, Defence R&D Canada, Ottawa, ON, Canada. e-mail: rajiv.sithiravel@drdc-rddc.gc.ca, mike.mcdonald@drdc-rddc.gc.ca and bhashyam.balaji@drdc-rddc.gc.ca

T.Kirubarajan is with the Department of Electrical and Computer Engineering, McMaster University, Hamilton, ON, L8S 4K1, Canada. e-mail: kiruba@mcmaster.ca

system model [24] and avoids degeneracy by modeling the PHD in continuous space. The nonlinearity of the state evolution or measurement model is naturally handled by the SPHD filter [24]. The SPHD filter is not limited to Gaussian systems. To extend the application of the SPHD filter to maneuvering multitarget tracking problems, a multimodal version, called the Multiple Model (MM) Spline Probability Hypothesis Density (MM-SPHD) filter, is derived in this paper.

The best choice for implementing multiple model estimation is the Interacting Multiple Model (IMM) [1] estimator and the IMM is a suboptimal filter that has been shown to be one of the most cost-effective state estimation schemes. Note, the standard IMM estimator assumes that the densities are Gaussian where the mode-dependent PHD filter is not. Therefore, the integration of the IMM estimator into mode-dependent PHD filter algorithm is not preferred here. Note, the IMM estimator uses only the first and the second order statistics to estimates the states, but for multimodal multitarget state problems cannot be approximated using the IMM estimator due to densities can be multimodal when they represent multitarget states. Therefore, the multiple model implementation used here adopts a method similar to the one used in the MM-PHD [20] filter. This new MM-SPHD filter not only works well for tracking maneuvering targets, but also inherits all the capabilities of the SPHD filter [24].

This paper presents the MM-SPHD filter derivations with details on the estimation of maneuvering multitarget state and the extraction of corresponding individual target states. The multidimensional multitarget system state transition model of the MM-SPHD filter is represented by tensor products of splines. The corresponding analytical state prediction and posterior density equations are derived. A preliminary version of our MM-SPHD filter was presented earlier in [25]. Simulation results in [25] showed that the MM-SPHD filter is a viable alternative to the multimodal GM-USMC-PHD, GM-SMC-PHD and the AP-PHD filters. The MM-SPHD filter inherits the performance characteristics of the single model SPHD filter [24]. Compared with our preliminary work [25], this journal version further analyses the stability and an optimal solution for knot placement. The optimal solution of knots results in superior estimation accuracy. In addition, more extensive simulation results to quantify the performance of the proposed work are also presented. Simulation results reveal that the MM-SPHD filter works efficiently and increased measurement noise levels do not destabilize it whereas other MM implementation suffer at higher noise levels. The MM-SPHD filter can maintain highly accurate tracks by taking advantage of dynamic knot movement [24], but at the expense of higher computational complexity.

The structure of this paper is as follows: Sections II and III briefly review the introduction to PHD filters and multiple model PHD filters, respectively. The B-spline and its properties are reviewed in Section IV. The proposed MM-SPHD filter formulations are presented in Section V for the multidimensional case with tensor products and two new knot selection schemes. Simulation results and conclusions are given in Sections VI and VII, respectively.

II. Introduction to PHD Filter

Maneuvering multitarget tracking algorithms face target motion model uncertainties and to overcome these uncertainties, most multitarget filters adopt multiple model estimation techniques [12,20]. Thus, multimodal estimators run each filter in their mode set using the same measurement assuming that the target state evolves according to one of r models in its mode set at any time and fuses the output of those filters to find an overall estimate [12].

Let ϑ_k be the number of targets at time k in multitarget state space $\mathcal{E}_s$. Then the multimodal multitarget state at time k can be written as

$$X_k \quad = \quad \{\mathbf{x}_{1,k}^{\mathbf{M}_k}, \ldots, \mathbf{x}_{\vartheta_k,k}^{\mathbf{M}_k}\} \in \mathcal{E}_s \tag{1}$$

where $\mathbf{x}_{l,k}^{\mathbf{M}_k}$ denotes the mode-dependent l-th target state vector at time k and $l \in \{1, \ldots, \vartheta_k\}$. Note that the order in which the multitarget states are listed has no significance in the Random Finite Set (RFS) multitarget model formulation. In the above, $\mathbf{M}_k \in \{1, \ldots, \mathsf{r}\}$ is the mode index parameter, where r is the number of possible models, and the mode index parameter is governed by an underlying Markov process with mode transition probability

$$\pi_{\mathfrak{p}\mathfrak{q}} = P(\mathbf{M}_k = \mathfrak{q} | \mathbf{M}_{k-1} = \mathfrak{p}) \quad \mathfrak{p}, \mathfrak{q} = 1, 2, \ldots, \mathsf{r} \tag{2}$$

The mode transition probability $\pi_{\mathfrak{p}\mathfrak{q}}$ can be assumed time-invariant and independent of the multitarget state. The state of the l-th target is given by

$$\mathbf{x}_{l,k} \quad = \quad f_{k,\mathbf{M}_k}(\mathbf{x}_{l,k-1}, \nu_{k,\mathbf{M}_k}, \mathbf{M}_k) \tag{3}$$

where at time k $\mathbf{x}_{l,k}$ denotes the l-th target state, the mode-dependent i.i.d. process noise sequence is denoted as $\nu_{k,\mathbf{M}_k}$ and $f_{k,\mathbf{M}_k}(\cdot)$ is the mode-dependent nonlinear system transition function.

Let $Z^{(k)} = \{Z_0, Z_1, \ldots, Z_k\} \in \mathcal{E}_o$ be the cumulative sets of measurements from time 0 to time k and assume that η_k denotes the number of target-originated measurements at time k. Measurements also consist of observations generated by the false alarm process and assume ϖ_k denotes the number of false measurements at time k. Then the set of measurements at time k in observation space $\mathcal{E}_o$ is given by

$$Z_k \quad = \quad \{\mathbf{z}_{1,k}, \ldots, \mathbf{z}_{\eta_k,k}\} \bigcup \{\mathbf{c}_{1,k}, \ldots, \mathbf{c}_{\varpi_k,k}\} \in \mathcal{E}_o \tag{4}$$

where the l-th target-originated measurement is given by

$$\mathbf{z}_{l,k} \quad = \quad h_{k,\mathbf{M}_k}(\mathbf{x}_{l,k}, \omega_{k,\mathbf{M}_k}, \mathbf{M}_k) \tag{5}$$

and $\omega_{k,\mathbf{M}_k}$ denotes the mode-dependent i.i.d. measurement noise with known statistics and $h_{k,\mathbf{M}_k}$ is a mode-dependent nonlinear function. The false measurements $\mathbf{c}_{i,k}$ are assumed to be uniformly distributed and their number ϖ_k is Poisson-distributed. Let $P_{\mathfrak{d},k}$ denote the probability of detection, thus the probability of $Z_k(\mathbf{x}_{i,k}^{\mathbf{M}_k}) = \mathbf{z}_{i,k} = \emptyset$ (i.e., the i-th target is not detected) is $1 - P_{\mathfrak{d},k}$. The average number of measurement is $\beth_k = \eta_k + \varpi_k^{'}$, where $\varpi_k^{'}$ is the average number of false alarms.

There are ϑ_k targets in state space $\mathcal{E}_s$ at time k and these targets can continue to exist, spawn new targets or terminate. In addition, new targets are born independently of already-existing targets. The number of targets and their states are unknown and, with maneuvering targets, the dynamic model of a target at any time is also unknown. That is, there are two unknown discrete random variables (i.e., number of targets and mode index of each target) and a continuous random variable (i.e., target state of each target) to be estimated at each time. From the observation space $\mathcal{E}_o$, $\beth_k$ measurements are received at time k. The origins of the measurements are not known, and thus the order in which they appear bears no significance. The measurements can also originate from clutter and false alarms.

At time k, the dynamic models of all targets and the dimension of the multitarget state X_k are unknown and time-varying. In the absence of model uncertainty, the randomness in the set can be characterized by modeling the multitarget states and

multitarget measurements as random finite set Ξ_k and $\aleph_k$ respectively. Given the realization X_{k-1} of Ξ_{k-1} at time k-1, the multitarget states at time k can be modeled by the RFS as

$$\Xi_k \quad = \quad S_k(X_{k-1}) \cup B_k(X_{k-1}) \cup \Gamma_k \tag{6}$$

where $S_k(X_{k-1})$ denotes the surviving targets and $B_k(X_{k-1})$ denotes the spawned targets. In addition, Γ_k denotes the newborn targets and these newborn targets are born independently from the surviving targets. Similarly, given a realization of X_k of $\aleph_k$, the multitarget measurement can be modeled by the RFS as

$$\aleph_k \quad = \quad \Phi_k(X_k) \cup C_k \tag{7}$$

where $\Phi_k(X_k)$ denotes the RFS measurement generated by X_k and C_k denotes measurement generated by clutter.

Let $p_{k-1|k-1}(X_{k-1}|Z^{(k-1)})$ denote the multitarget prior density of the system dynamic model at time $k-1$. Then, the prediction and update steps of the optimal multitarget Bayes filter recursion are given by [1]

$$\begin{aligned} p_{k|k-1}(X_k|Z^{(k-1)}) \quad = \quad & \int p_{k|k-1}(X_k|X_{k-1}) \\ & \cdot p_{k-1|k-1}(X_{k-1}|Z^{(k-1)}) \\ & \cdot \mu_s(dX_{k-1}) \end{aligned} \tag{8}$$

$$p_{k|k}(X_k|Z^{(k)}) \quad = \quad \frac{g_k(Z_k|X_k)p_{k|k-1}(X_k|Z^{(k-1)})}{\int g_k(Z_k|X_k)p_{k|k-1}(X_k|Z^{(k-1)})\mu_s(dX_k)} \tag{9}$$

respectively, where $p_{k|k-1}(X_k|X_{k-1})$ is the multitarget dynamic model transition density, $g_k(Z_k|X_k)$ denotes the multitarget likelihood and μ_s takes the place of Lebesgue measure. The posterior density $p_{k|k}(X_k|Z^{(k)})$ can be determined using (9).

In order to get a multiple model PHD filter, in [15,20], it is assumed that there are r dynamic models and each target evolves according to one of them at time $k-1$. Furthermore, from time $k-1$ to time k, the target can switch from model $\mathfrak{p}$ to model $\mathfrak{q}$ with probability $\pi_{\mathfrak{q}|\mathfrak{p}} = \pi_{\mathfrak{p}\mathfrak{q}} = P(\mathbf{M}_k = \mathfrak{q}|\mathbf{M}_{k-1} = \mathfrak{p})$. Then, a multimodal state space of the form

$$\mathfrak{X} = \bigcup_{i=1}^{\mathsf{r}} \mathfrak{X}_i \tag{10}$$

is considered for the target dynamic state evolution. The state vector in $\mathfrak{X}$ is $\mathbf{x}^e$ and, for $\mathbf{x}^e \in \mathfrak{X}_i$, it has the form $[\mathbf{x}^T \ i]^T$. Every target, no matter which dynamic model it follows, evolves in this hybrid space. The random state vector for a single target is represented as $[\mathbf{x}^T \ \mathbf{M}]^T$ where $\mathbf{M} \in \{1, \ldots, \mathsf{r}\}$. Here, $\mathbf{x}$ is the kinematic state vector of that target. On the other hand, $\mathbf{M}$ is a variable with integer value and $\mathbf{M} = i$ denotes the random event that the target is evolving according to the i-th dynamic model at time $k-1$. It should be noted that the single target state space for different dynamic models may be different, so the dimension of $\mathbf{x}$ depends on the type of dynamic model represented by $\mathbf{M}$. With the above state space model, given the targets following dynamic model i, these targets can only stay in space $\mathfrak{X}_i$ ($i = 1, \cdots, \mathsf{r}$).

For a real–valued function $f(\mathbf{x}^e)$ defined on $\mathfrak{X}$, its integration in a sub region $\mathfrak{S} \in \mathfrak{X}$ is given by

$$\int_{\mathfrak{S}} f(\mathbf{x}^e)d\mathbf{x}^e = \sum_{i=1}^{\mathsf{r}} \int_{\mathfrak{X}_i \bigcap \mathfrak{S}} f([\mathbf{x} \ i]^T)d\mathbf{x} \tag{11}$$

Correspondingly, for two real–valued functions f and g defined in space $\mathfrak{X}$, their inner product, $\langle f, g \rangle$, becomes

$$\langle f, g \rangle = \sum_{i=1}^{\mathsf{r}} \int_{\mathfrak{X}_i} f([\mathbf{x} \ i]^T)g([\mathbf{x} \ i]^T)d\mathbf{x} \tag{12}$$

In [15,20], the state transition for the k-th target is assumed to follow a jump Markov model:

$$f([\mathbf{x}_k, \mathfrak{q}]|[\mathbf{x}_{k-1}, \mathfrak{p}]) = \pi_{\mathfrak{q}|\mathfrak{p}} f(\mathbf{x}_k|[\mathbf{x}_{k-1}, \mathfrak{p}]) \tag{13}$$

In [15,20], except for the above jump Markov dynamic mode transition model, all the assumptions related to the target dynamic system and the measurement model are exactly same as those made in [14,32]. Thus, by substituting (11) and (12) into the PHD prediction–updating equations in [14,32], the equations for the MM–PHD prediction and update were obtained.

III. PHD Filter for Maneuvering Targets

As described in [20], a recursive MM-PHD filter algorithm has three main stages. Those three stages are mixing, prediction and update.

A. MM-PHD mixing

Assume that the mode-dependent prior density $D_{k-1|k-1}(\mathbf{x}_{k-1}, \mathbf{M}_{k-1} = \mathfrak{p}|Z^{(k-1)})$ is available at time $k-1$. Then using the total probability theorem the mode-dependent initial density can be defined as $\tilde{D}_{k|k-1}(\mathbf{x}_{k-1}, \mathbf{M}_k = \mathfrak{q}|Z^{(k-1)})$ can be determined as [20]

$$\tilde{D}_{k|k-1}(\mathbf{x}_{k-1}, \mathbf{M}_k = \mathfrak{q}|Z^{(k-1)}) = \sum_{\mathfrak{p}=1}^{\mathsf{r}} D_{k-1|k-1}(\mathbf{x}_{k-1}, \mathbf{M}_{k-1} = \mathfrak{p}|Z^{(k-1)}) \pi_{\mathfrak{p}\mathfrak{q}} \tag{14}$$

where $\mathfrak{q} = 1, \ldots, \mathsf{r}$, the number of filters is denoted by r and $\pi_{\mathfrak{p}\mathfrak{q}}$ denotes the Markovian model transition probability matrix. Note, the initial density fed to the PHD filter that is matched to motion model $\mathfrak{q}$. The target can spawn, die, or born and these are only considered in the prediction stage.

B. MM-PHD prediction

Assume that each target evolves and generates observations independently of one another. A target can continue to survive or disappear from the scene, can be spawned by already-existing targets, and also new targets can be born in the scene independently from the already-existing targets. The mode-dependent predicted density is determined as

$$\begin{aligned} D_{k|k-1}(\mathbf{x}_k, \mathbf{M}_k = \mathfrak{q}|Z^{(k-1)}) &= D_{\mathbf{c},k|k-1}(\mathbf{x}_k, \mathbf{M}_k = \mathfrak{q}) \\ &\quad + D_{\mathbf{s},k|k-1}(\mathbf{x}_k, \mathbf{M}_k = \mathfrak{q}) \\ &\quad + D_{\mathbf{nb},k}(\mathbf{x}_k, \mathbf{M}_k = \mathfrak{q}) \end{aligned} \tag{15}$$

where the mode-dependent predicted density of existing targets is expressed as follows:

$$\begin{aligned} D_{\mathbf{c},k|k-1}(\mathbf{x}_k, \mathbf{M}_k = \mathfrak{q}) &= \int P_{\mathfrak{s},k|k-1}(\mathbf{x}_{k-1}, \mathbf{M}_k = \mathfrak{q}) \\ &\quad \cdot p_{k|k-1}(\mathbf{x}_k, \mathbf{M}_k = \mathfrak{q}|\mathbf{x}_{k-1}, \mathbf{M}_{k-1} = \mathfrak{p}) \\ &\quad \cdot \tilde{D}_{k|k-1}(\mathbf{x}_{k-1}, \mathbf{M}_k = \mathfrak{q}|Z^{(k-1)}) \\ &\quad \cdot d\mathbf{x}_{k-1} \end{aligned} \tag{16}$$

where $p_{k|k-1}(\mathbf{x}_k, \mathbf{M}_k = \mathfrak{q}|\mathbf{x}_{k-1}, \mathbf{M}_{k-1} = \mathfrak{p})$ denotes a mode-dependent single Markov transition density of the state of existing-targets and $P_{\mathfrak{s},k|k-1}(\cdot)$ denotes the mode-dependent survival probability of existing targets that accounts for the event that a target with state $\mathbf{x}_{k-1}$ at time step $k-1$ will survive at time step k. The mode-dependent predicted density of spawned targets can be expressed as

$$\begin{aligned} D_{\mathbf{s},k|k-1}(\mathbf{x}_k, \mathbf{M}_k = \mathfrak{q}) &= \int \beta_{\mathbf{s},k|k-1}(\mathbf{x}_k, \mathbf{M}_k = \mathfrak{q}|\mathbf{x}_{k-1}, \mathbf{M}_{k-1} = \mathfrak{p}) \\ &\quad \cdot \tilde{D}_{k|k-1}(\mathbf{x}_{k-1}, \mathbf{M}_k = \mathfrak{q}|Z^{(k-1)}) \\ &\quad \cdot d\mathbf{x}_{k-1} \end{aligned} \tag{17}$$

where $\beta_{\mathbf{s},k|k-1}(\mathbf{x}_k, \mathbf{M}_k = \mathfrak{q}|\mathbf{x}_{k-1}, \mathbf{M}_{k-1} = \mathfrak{p})$ denotes the mode-dependent PHD of the new targets spawned by existing targets. The PHD of the mode-dependent likelihood function is $\beta_{\mathbf{s},k|k-1}(\mathbf{X}_k|\mathbf{M}_k = \mathfrak{q})$, which is the mode-dependent likelihood that a group of new targets with state set X_k will be spawned at time step k by a single target that had state $\mathbf{x}_{k-1}$ at time step $k-1$.

Appearance of completely new targets is also described by mode-dependent $\beta_{\mathbf{nb},k}(X_k, \mathbf{M}_k = \mathfrak{q})$, which is the mode-dependent likelihood that new targets with state set X_k will enter the scene at time step k and its PHD is $\beta_{\mathbf{nb},k}(\mathbf{x}_k, \mathbf{M}_k = \mathfrak{q})$. The mode-dependent predicted newborn target density $D_{\mathbf{nb},k}(.)$ depends on the system model. The expected number of targets in the surveillance region can be determined by finding the area of the mode-dependent predicted PHD $D_{k|k-1}(\mathbf{x}_k, \mathbf{M}_k = \mathfrak{q}|Z^{(k-1)})$.

C. MM-PHD update

The predicted density can be corrected with the available measurements $Z_k \in Z^{(k)}$ from observation space $\mathcal{E}_o$ at time step k to get the updated density with the assumption that no target generates more than one measurement. Each measurement is generated by no more than a single target and all measurements are conditionally independent of target state. The number of false alarm λ_k is Poisson distributed with spatial density $C_k(\mathbf{z}_k)$ with the assumption of standard multimodal multitarget measurement model from Section II.

At time step k the detection probability of a target with state $\mathbf{x}_k$ is defined as $P_{\mathfrak{d}}(\mathbf{x}_k, \mathbf{M}_k = \mathfrak{q})$ and the mode-dependent updated PHD at scan k can be determined as (for $\mathfrak{q} = 1, \ldots, \mathfrak{r}$)

$$\begin{aligned} D_{k|k}(\mathbf{x}_k, \mathbf{M}_k = \mathfrak{q}|Z^{(k)}) &\cong (1 - P_{\mathfrak{d},k}(\mathbf{x}_k, \mathbf{M}_k = \mathfrak{q}))D_{k|k-1}(\mathbf{x}_k, \mathbf{M}_k = \mathfrak{q}|Z^{(k-1)}) \\ &\quad + \sum_{\mathbf{z}_k \in Z_k} \frac{\phi_k(\mathbf{z}_k|Z^{(k-1)}, \mathbf{M}_k = \mathfrak{q})}{\lambda_k C_k(\mathbf{z}_k) + \int \phi_k(\mathbf{z}_k|Z^{(k-1)}, \mathbf{M}_k = \mathfrak{q})d\mathbf{x}_k} \end{aligned} \tag{18}$$

where the function $\phi_k(.)$ is given as

$$\begin{aligned} \phi_k(\mathbf{z}_k|Z^{(k-1)}, \mathbf{M}_k = \mathfrak{q}) &= P_{\mathfrak{d},k}(\mathbf{x}_k, \mathbf{M}_k = \mathfrak{q}) \\ &\quad \cdot p_{k|k}(\mathbf{z}_k|\mathbf{x}_k, \mathbf{M}_k = \mathfrak{q}) \\ &\quad \cdot D_{k|k-1}(\mathbf{x}_k, \mathbf{M}_k = \mathfrak{q}|Z^{(k-1)}) \end{aligned} \tag{19}$$

By finding the area of the mode-dependent updated PHD $D_{k|k}(.)$ one can determine the average number of targets as

$$\hat{N}_{k|k}^{\mathbf{M}_k = \mathfrak{q}} = \int D_{k|k}(\mathbf{x}_k, \mathbf{M}_k = \mathfrak{q}|Z^{(k)})d\mathbf{x}_k \tag{20}$$

and the total number of estimated targets as

$$\hat{N}_{k|k} \quad = \quad \sum_{\mathfrak{q}=1}^{\mathfrak{r}} \hat{N}_{k|k}^{\mathbf{M}_k=\mathfrak{q}} \tag{21}$$

IV. B-SPLINES

A brief background on B-spline is provided in this section. For further details, readers can refer to [4]. A p-th order B-spline curve $\mathbf{C}(x)$ of a certain variable x (e.g., multitarget state) is defined as

$$\mathbf{C}(x) \quad = \quad \sum_{i=1}^{n_s} \mathbb{P}_i B_{i,p,\mathbf{t}}(x) \qquad 2 \leq p \leq n_s, \tag{22}$$

where $\mathbb{P}_i$ is the i-th control point and n_s denotes the total number of control points. The B-spline blending functions or basis functions are denoted by $B_{i,p,\mathbf{t}}(x)$. Blending functions are polynomials of degree $p-1$. The order p can be chosen from 2 to n_s and the continuity of the curve can be kept by selecting $p \geq 3$. The knot denoted by $\mathbf{t}$ is a $1 \times \tau$ vector and $\mathbf{t}$ is a non-decreasing sequence of real numbers, where $\mathbf{t} = \{t_1, \ldots, t_\tau\}$, i.e., $t_i \leq t_{i+1}$, $i = 1, \ldots, \tau$. The knot vector relates the parameter x to the control points. Note, one can control over the shape of any curve by adjusting the locations of the control points.

The i-th basis function can be defined as [6]

$$B_{i,p}(x) \quad = \quad \frac{(x - t_i)B_{i,p-1}(x)}{t_{i+p-1} - t_i} + \frac{(t_{i+p} - x)B_{i-1,p-1}(x)}{t_{i+p} - t_{i+1}} \tag{23}$$

where, $t_i \leqslant x < t_{i+p}$ and

$$B_{i,1}(x) = \begin{cases} 1 & \text{if } \ t_i \leqslant x < t_{i+1}, \\ 0 & \text{otherwise.} \end{cases} \tag{24}$$

where variables t_is in (23) are denote knot elements. The basis function $B_{i,p,\mathbf{t}}(x)$ is non-zero in the interval $[t_i, t_{i+p}]$. The basis function $B_{i,p}$ can have the form $0/0$ and assume $0/0 = 0$. For any value of the parameter, x, the sum of the basis functions is one, i.e.,

$$\sum_{i=1}^{n_s} B_{i,p}(x) = 1, \tag{25}$$

Unidimensional splines can be extended to multidimensional ones through the use of tensor product spline construction [4]. A spline subspace $B_{i_j,p_j,t_j}(x_j)$ is defined for each dimension where x_j denotes the variable in the j-th dimension. Thus, the spline representation of a multidimensional function $\mathbf{C}(x_1, \ldots, x_m)$ is given as

$$\mathbf{C}(x_1, \ldots, x_m) = \sum_{i_1}^{n_s} \cdots \sum_{i_m}^{n_s} \mathbb{P}_{i_1,\ldots,i_m} B_{i_1,p_1,\mathbf{t}_1}(x_1) \ldots B_{i_m,p_m,\mathbf{t}_m}(x_m) \tag{26}$$

Similar to the unidimensional case, the construction of the above multidimensional spline polynomials can be done by solving a corresponding set of linear equations.

Generally, for a given basic sequence of B-splines $\{B_{i,p,\mathbf{t}}\}_{i=1}^{n_s}$ and strictly increasing sequence of data series $\{x_j\}_{j=1}^{n_s}$, the B-spline interpolation function $\hat{c}(x)$ can be written as

$$\hat{c}(x) \quad = \quad \sum_{i=1}^{n_s} \mathbb{P}_i B_{i,p,\mathbf{t}}(x) \tag{27}$$

where $\hat{c}(x)$ agrees with function $c(x)$ at all x_j if and only if

$$\sum_{i=1}^{n_s} \mathbb{P}_i B_{i,p,\mathbf{t}}(x_j) \quad = \quad c(x_j), \qquad \text{for} \quad j = 1, \ldots, n_s \tag{28}$$

In fact, (28) is a linear system of n_s equations with n_s unknown values of $\mathbb{P}_i$ and the i-th row and j-th column of the coefficient matrix equals $B_{i,p,\mathbf{t}}(x_j)$, which implies that the spline interpolation function can be found by solving a set of linear system equations [6]. The coefficient matrix can be verified for invertibility using the Schoenberg-Whitney theorem [22].

A. Use of B-Splines

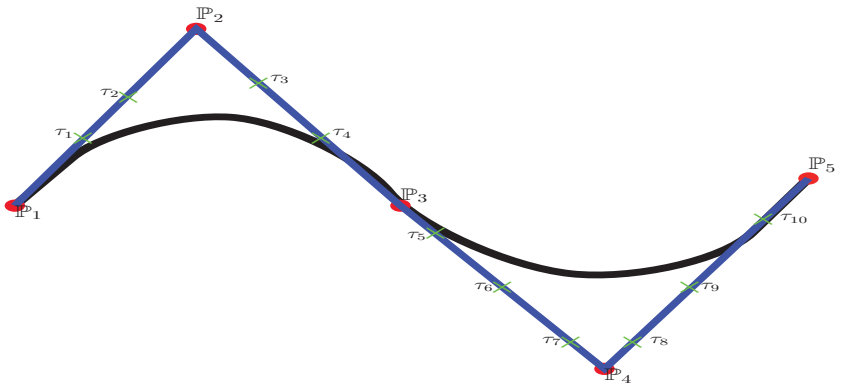

Fig. 1. B-spline approximation (black curve: original function, blue line: B-spline approximation, red dots: control points, green crosses: knots).

The B-spline transformation can be applied to single and multidimensional statistical functions, e.g., probability density function and probability hypothesis density function, without the any assumption on noises [6, 22]. As shown in Figure 1, for a given curve (black solid line), a B-Spline representation can be defined by set of control points $[\mathbb{P}_i]_{i=1}^{5}$ (red dots). The movement of any control point will affect the curve and the effect can be on the entire curve (global effect) or in a certain part of the curve (local effect). The primary benefit of using B-spline is its local controllability. Note that the range on the curve where the control point movement affects is divided into small segments (green crosses) called knots. The total number of knots is always greater than the total number of control points. Adding or removing knots using appropriate control point movement can exactly replicate the function/curve, which is suitable for implementing filtering algorithms using splines [19, 24]. Also, a higher order (3 or more) B-spline curve tends to be smooth and maintains the continuity of the curve. The continuity of the B-spline curve enables continuous state estimation [19, 24]. As shown in Figure 2, control points will get closer to the curve if it is redefined by inserting knots into the curve and thereby increasing the vertices. With increasing number of knots and adjusting the control points accordingly, the control polygon converges to the curve.

The B-spline transformation can be derived using the spline approximation curve (SAC) method [22] or the spline interpolation curve (SIC) method [22]. The difference between these two spline transformations is that the SAC does not necessarily pass through all control points, but must go through the first and the last ones. In contrast, the SIC must pass through all control points. The B-spline uses the SIC implementation. Note that the B-spline implementation used here is the standard one, but there are many other more complex options like Cubic Spline, Weighted Spline, Nu-spline, Beta Splines, Sigma Splines and Hermite Splines [23]. B-spline based target tracking can handle a continuous state space, makes no special assumption on the noises, and is able accurately approximate arbitrary probability density or probability hypothesis density surfaces. In most

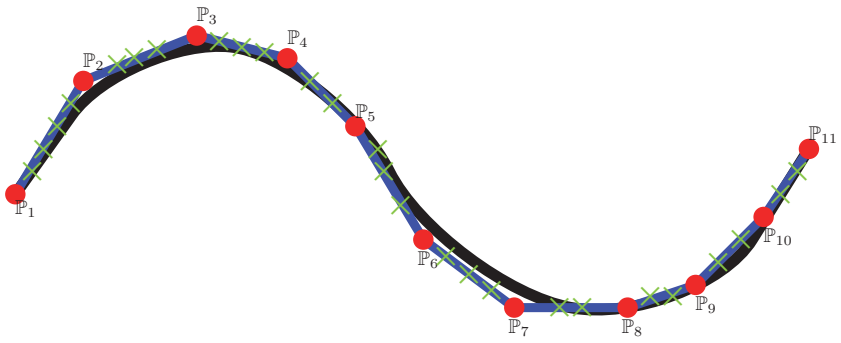

Fig. 2. B-spline approximation with redefined knot vector (black curve: original function, blue line: B-spline approximation, red dots: control points, green crosses: knots).

tracking algorithms, during the update stage, the states are updated, but in B-spline based target tracking only the knots are updated [10, 19, 24].

B. Properties of B-splines

1) Differential of a B-spline:

$$\mathfrak{D}(\sum_{i=1}^{n_s} \mathbb{P}_i B_{i,p,\mathbf{t}}(x)) \quad = \quad (p-1)\sum_{i=1}^{n_s+1} \frac{\mathbb{P}_i - \mathbb{P}_{i-1}}{t_{i+p-1} - t_i} B_{i,p-1,\mathbf{t}}(x) \tag{29}$$

where $\mathfrak{D}(\cdot)$ denotes the differential operator, and both $\mathbb{P}_0$, and $\mathbb{P}_{n_s+1}$ are zeros.

2) Integral of a B-spline: The integral of a B-spline over the interval $[t_1, x]$ $(t_1 \leq x \leq t_s)$ is given by

$$\int_{t_1}^{x} \sum_{i=1}^{n_s} \mathbb{P}_i B_{i,p}(c)dc \quad = \quad \sum_{i=1}^{s-1} (\sum_{j=1}^{i} \mathbb{P}_j (t_{j+p} - t_j)/p) B_{i,p+1}(x) \tag{30}$$

3) Positivity property: The B-spline $B_{i,p,\mathbf{t}}$ is a combination of at most p nontrivial polynomial pieces and becomes insignificant outside the interval $[t_i, ..., t_{i+p}]$ and $[t_i, ..., t_{i+p}] > 0$ [6]. That is,

$$B_{i,p,\mathbf{t}}(x) > 0, \qquad t_i < x < t_{i+p} \tag{31}$$

while

$$B_{i,p,\mathbf{t}}(x) = 0 \quad \text{for} \quad t_i = t_{i+p} \tag{32}$$

Note, the spline representation of probability densities and likelihood functions all can be positive, since $\mathbb{P}_i \geq 0$ for all i.

4) Knot insertion property: Knots can be inserted additionally as described in [22] and a new knot sequence $\hat{\mathbf{t}}$ can be obtained by inserting one element, say x into an already existing knot sequence $\mathbf{t}$, then for any function $c \in \Psi$

$$\sum_i \mathbb{P}_i B_{i,p,\mathbf{t}}(x) \quad = c(x) = \quad \sum_i \hat{\mathbb{P}}_i B_{i,p,\hat{\mathbf{t}}}(x) \tag{33}$$

with

$$\hat{\mathbb{P}}_i = (1 - \hat{w}_{i,p}(x))\mathbb{P}_{i-1} + \hat{w}_{i,p}(x)\mathbb{P}_i \quad \text{for all } i \tag{34}$$

where Ψ is the span of $B_{i,p,\mathbf{t}}(x)$ and $\hat{w}_{i,p}(x) = \frac{x - \hat{t}_i}{\hat{t}_{i+p-1} - \hat{t}_i}$.

5) Knot removal property: Knot removal is the reverse process of knot insertion. Let

$$c(x) \quad = \quad \sum_{i=1}^{n_s} \mathbb{P}_i B_{i,p,\mathbf{t}}(x) \tag{35}$$

be defined on x, and let t_e be an interior knot of multiplicity s in $\mathbf{t}$; end knots are not removed. The size of the knot vector is $\tau = \|\mathbf{t}\|$, $e \in \{p, \ldots, \tau - p\}$ and $1 \leq s \leq p$. Let $\mathbf{t}_r$ denote the knot vector obtained by removing t_e r times from $\mathbf{t}(e \leq r \leq s + e)$. Note that t_e is r times removable if $c(x)$ has a precise representation of the form [22]

$$c(x) \quad = \quad \sum_{i=1}^{n_s - r} \mathbb{Q}_i \hat{B}_{i,p,\mathbf{t}_r}(x) \tag{36}$$

where $\hat{B}_{i,p,\mathbf{t}_r}(x)$ are the basis functions on $\mathbf{t}_r$. That is, (35) and (36) geometrically and parametrically represent the same curve. Hence, the knot t_e is r times removable if and only if the curve $c(x)$ is C^{p-s+r} continuous at $t_e s$. The new control points denoted by $\mathbb{Q}_i$ can be determined as described in [22]. Thus, the equations for removing t_e r-th time are

$$\mathbb{Q}_i = \begin{cases} \mathbb{Q}^r_{i=k} = \frac{\mathbb{Q}^{r-1}_k - (1-\alpha_k)\mathbb{Q}^r_{k-1}}{\alpha_k} & (e-p-r+1) \leq k \leq 0.5(2e-p-s-r), \\ \mathbb{Q}^r_{i=j} = \frac{\mathbb{Q}^{r-1}_j - \alpha_j \mathbb{Q}^r_{j+1}}{(1-\alpha_j)} & 0.5(2e-p-s+r+1) \leq j \leq (e-s+r-1), \end{cases} \tag{37}$$

with

$$\alpha_k \quad = \quad \frac{t - t_k}{t_{k+p+r} - t_k} \tag{38}$$

and

$$\alpha_j \quad = \quad \frac{t - t_{j-r+1}}{t_{j+p+1} - t_{j-r+1}} \tag{39}$$

6) Schoenberg-Whitney theorem: Let $\mathbf{t}$ be a knot vector, p and n be integers such that $n > p > 0$, and suppose x is strictly increasing with $n+1$ elements. Then matrix $L_{ij} = B_{i,p,\mathbf{t}}(x_j)$ from (28) is invertible if and only if $B_{i,p,\mathbf{t}}(x_i) \neq 0$, $i = 0, \ldots, n$, i.e., if and only if $t_i < x_i < t_{i+p+1}$, for all i [22].

V. MM-SPHD FILTERING

The proposed MM-SPHD filter implementation is based on the SPHD filter's extension to multiple model estimation. This section derives the MM-SPHD filter for the multidimensional multitarget state space models. Let a multidimensional multitarget system state at time k be denoted as $X_k = \{\mathbf{x}_{1,k}, \ldots, \mathbf{x}_{\vartheta_k,k}\}$ where each target has multidimensional state $\mathbf{x}_k = [\mathbf{x}^1_k, \ldots, \mathbf{x}^n_k]'$ and n denotes the number of dimensions.

A. MM-SPHD mixing

The MM-SPHD filter derivations follow Section III. Let the initial MM-SPHD be

$$\begin{aligned} \tilde{\mathbf{B}}_{k|k-1}(\mathbf{x}_{k-1}, \mathbf{M}_k = \mathfrak{q}) \quad = \quad & \sum_{i_1}^{n_s} \cdots \sum_{i_n}^{n_s} \mathbb{P}_{i_1,\ldots,i_n} \\ & \cdot B_{i_1,p,\mathbf{t}^1_{k-1}}(\mathbf{x}^1_{k-1}, \mathbf{M}_k = \mathfrak{q}) \ldots \\ & \cdot B_{i_n,p,\mathbf{t}^n_{k-1}}(\mathbf{x}^n_{k-1}, \mathbf{M}_k = \mathfrak{q}) \end{aligned} \tag{40}$$

where $\tilde{\mathbf{B}}_{k|k-1}(\mathbf{x}_{k-1}, \mathbf{M}_k = \mathfrak{q})$ denotes the $\mathfrak{q}$-th mode-dependent initial multitarget multidimensional MM-SPHD and $\mathbf{M}_k \in \{1, \ldots, \mathfrak{r}\}$ is the model index at time k, where $\mathfrak{r}$ denotes the total number of models. The number of dimensions is denoted by n

and $\mathfrak{i} = i_1, \ldots, i_n$. The number of knots for all dimensions is the same at τ. The n dimensional knot $\mathbf{t}_{k-1} = \{\mathbf{t}^1_{k-1}, \ldots, \mathbf{t}^n_{k-1}\}$, is an $n \times \tau$ array. Each row vector of $\mathbf{t}_{k-1}$ consists of a set of prior knots $\mathbf{t}^l_{k-1} = \{t^l_{1,k-1}, \ldots, t^l_{\tau,k-1}\}$ where $l = 1, \ldots, n$. Assume that the l-th dimensional prior knot $\mathbf{t}^l_{k-1}$ represents a parametric curve in the range $[a, b]$ of order p (degree$= p-1$) with n_s input/control points. Then, the knot vector will have $\tau = n_s + p$ elements. The knot elements can be determined using the uniform knot selection method as [6]

$$\mathbf{t}^l_{k-1} = \begin{cases} t^l_{1,k-1}, \ldots, t^l_{p,k-1} = a \\ t^l_{i+p,k-1} = a + \frac{i(b-a)}{n_s+p-1} \quad \text{for} \quad i = 1, \ldots, (n_s - p) \\ t^l_{\tau-p,k-1}, \ldots, t^l_{\tau,k-1} = b \end{cases} \tag{41}$$

Alternatively, the knot elements can be created using average knot selection by averaging the parameter values ($x_i,\ i = 1, \ldots, (n_s - p)$) in their neighborhood given parametrization $\mathbf{x}^l_k = x_1, \ldots, x_{n_s}$ as [6]

$$\mathbf{t}^l_{k-1} = \begin{cases} t^l_{1,k-1}, \ldots, t^l_{p,k-1} = a \\ t^l_{i+p,k-1} = \frac{1}{p}\sum_{j=i}^{i+p-1} x_j \quad \text{for} \quad i = 1, \ldots, (n_s - p) \\ t^l_{\tau-p,k-1}, \ldots, t^l_{\tau,k-1} = b \end{cases} \tag{42}$$

or one can use the optimal knot selection, which is an iterative method proposed in [6]. This method does not consider the location of the input/control points for the optimization. The Matlab function *optknt* can be used to produce this knot vector.

The n dimensional control point set or coefficient matrix is denoted by $\mathbb{P}_{\mathfrak{i}}$. The number of control points is denoted by n_s and its same for all dimensions. Note that the number of knots must be greater than the number of control points.

The initial MM-SPHD $\tilde{\mathbf{B}}_{k|k-1}(\mathbf{x}_{k-1}, \mathbf{M}_k = \mathfrak{q})$ matched to multitarget model $\mathfrak{q}$ is sent to the MM-SPHD filter. The initial MM-SPHD $\tilde{\mathbf{B}}_{k|k-1}(\cdot)$ can be calculated on the basis of the Markovian model transition probability matrix $\pi_{\mathfrak{p}\mathfrak{q}}$ and mode-dependent multitarget multidimensional prior MM-SPHD $\mathbf{B}_{k-1|k-1}(\mathbf{x}_{k-1}, \mathbf{M}_{k-1} = \mathfrak{p})$. That is,

$$\begin{aligned} \tilde{\mathbf{B}}_{k|k-1}(\mathbf{x}_{k-1}, \mathbf{M}_k = \mathfrak{q}) &= \sum_{\mathfrak{p}=1}^{\mathfrak{r}} \mathbf{B}_{k-1|k-1}(\mathbf{x}_{k-1}, \mathbf{M}_{k-1} = \mathfrak{p}) \\ &\quad \cdot \pi_{\mathfrak{p}\mathfrak{q}} \qquad \mathfrak{q} \in \{1, \ldots, \mathfrak{r}\} \end{aligned} \tag{43}$$

where the prior MM-SPHD of the $\mathfrak{p}$-th dynamic system can be determined as

$$\begin{aligned} \mathbf{B}_{k-1|k-1}(\mathbf{x}_{k-1}, \mathbf{M}_{k-1} = \mathfrak{p}) &= \sum_{g_1}^{n_s} \cdots \sum_{g_n}^{n_s} \mathbb{P}_{g_1,\ldots,g_n} \\ &\quad \cdot B_{g_1,p,\mathbf{t}^1_{k-1}}(\mathbf{x}^1_{k-1}, \mathbf{M}_{k-1} = \mathfrak{p}) \ldots \\ &\quad \cdot B_{g_n,p,\mathbf{t}^n_{k-1}}(\mathbf{x}^n_{k-1}, \mathbf{M}_{k-1} = \mathfrak{p}) \end{aligned} \tag{44}$$

and $\mathfrak{p} = \{1, \ldots, \mathfrak{r}\}$. For all $\mathfrak{r}$ system models, the prior MM-SPHD $\mathbf{B}_{k-1|k-1}(\cdot)$ are summed together with scaling by the corresponding mode probability $\pi_{\mathfrak{p}\mathfrak{q}}$ to determine the initial MM-SPHD $\tilde{\mathbf{B}}_{k|k-1}(.)$ as in (43). The prior number of expected targets is the integral of $\tilde{\mathbf{B}}_{k|k-1}(\mathbf{x}_{k-1}, \mathbf{M}_k = \mathfrak{q})$ over the region of state space $\mathcal{E}_s$ for the $\mathfrak{q}$-th model evaluated as

$$\hat{N}^{\mathfrak{q}}_{k-1|k-1} = \int_{\mathcal{E}_s} \tilde{\mathbf{B}}_{k|k-1}(\mathbf{x}_{k-1}, \mathbf{M}_k = \mathfrak{q}) d\mathbf{x}_{k-1} \tag{45}$$

where $\mathfrak{q} = \{1, \ldots, \mathfrak{r}\}$. Using (45), the prior number of expected targets can be determined for all the models. Then the overall prior number of expected targets can be determined as

$$\hat{N}_{k-1|k-1} = \sum_{\mathfrak{q}=1}^{\mathfrak{r}} \hat{N}^{\mathfrak{q}}_{k-1|k-1} \tag{46}$$

The target can spawn, die or born and these events only considered at the prediction stage.

B. MM-SPHD prediction

The mode-dependent multitarget state transition density's spline representation is a $2n$-dimensional function determined using system model (3) as

$$\begin{aligned} p_{k|k-1}(\mathbf{x}_k, \mathbf{M}_k = \mathfrak{q}|\mathbf{x}_{k-1}, \mathbf{M}_{k-1} = \mathfrak{p}) \quad = \quad & \sum_{j_1} \dots \sum_{j_{2n}} \mathbb{P}_{j_1,\dots,j_{2n}} \\ & \cdot B_{j_1,\mathbf{t}_k^1}(\mathbf{x}_k^1, \mathbf{M}_k = \mathfrak{q}) \dots \\ & \cdot B_{j_n,\mathbf{t}_k^n}(\mathbf{x}_k^n, \mathbf{M}_k = \mathfrak{q}) \\ & \cdot B_{j_{n+1},p,\mathbf{t}_{k-1}^1}(\mathbf{x}_{k-1}^1, \mathbf{M}_{k-1} = \mathfrak{p}) \dots \\ & \cdot B_{j_{2n},p,\mathbf{t}_{k-1}^n}(\mathbf{x}_{k-1}^n, \mathbf{M}_{k-1} = \mathfrak{p}) \end{aligned} \tag{47}$$

where $\mathfrak{q}, \mathfrak{p} \in \{1, \dots, \mathfrak{r}\}$, $\mathfrak{j} = \{j_1, \dots, j_{2n}\}$ and $\mathbf{t}_k$ denotes an $n \times \tau$ knot array at time k and it consists of row vectors $\mathbf{t}_k^1, \dots, \mathbf{t}_k^n$. Each row vector of $\mathbf{t}_k$ consists of a set of predicted knots $\mathbf{t}_k^l = \{t_{1,k}^l, \dots, t_{\tau,k}^l\}$ where $l = 1, \dots, n$. For a multidimensional system, the selection of predicted knots becomes challenging and a suboptimal low-complexity method is used to calculate the predicted knots. At time $k-1$, from (45) one can determine the mode-dependent prior number of targets and their states by using the K-means clustering algorithm [28]. An alternative is the Expectation-Maximization (EM) based peak extraction approach [29]. For example, assume that there are ϑ_{k-1} targets at $k-1$ and their states are

$$\mathbf{x}_{h_{k-1},k-1} \quad = \quad [\mathbf{x}_{h_{k-1},k-1}^1, \dots, \mathbf{x}_{h_{k-1},k-1}^n]' \qquad h_{k-1} \in 1, 2, \cdots, \vartheta_{k-1} \tag{48}$$

Note that the l-th dimension knot vector $\mathbf{t}_{k-1}^l$ has $\tau = \tau_l$ knot elements and each dimension has τ elements in the corresponding knot vector. Next, we can find the l-th dimensional prior knot elements that approximate the l-th dimensional state parameters as

$$t_{\zeta_{h_{k-1}},k-1}^l \quad \approx \quad \mathbf{x}_{h_{k-1},k-1}^l \qquad h_{k-1} \in 1, 2, \cdots, \vartheta_{k-1} \tag{49}$$

where $\zeta_{h_{k-1}} \in (1, \dots, \tau)$. Using the locations of $\zeta_1, \cdots, \zeta_{\vartheta_{k-1}}$ one can interactively shape the B-spline curve: knot elements can be added to $\mathbf{t}_{k-1}^l$ as in Section (IV-B4) to increase the number of control points that can be modified. When control points are moved, the level of continuity at the knots can increase or decrease. Knot removal as in Section (IV-B5) can be invoked in order to obtain the most compact representation of the curve. Knot removal can also be used to remove unnecessary knots. Note that the first and the last knot elements are never removed. This method can be used for all dimensions. Then, $\prod_l \tau_l$ different sample vectors $\mathbf{\Psi}_{k-1,t}$ are formed by selecting a single knot $t_{e_l,k-1}^l$ from the respective dimensional set of knots $\mathbf{t}_{k-1}^l$ and this is done for each dimension $e_l = 1, \dots, \tau$. In the n-dimensional case, the collection of all such sample vectors is $\mathbf{\Psi}_{k-1,t} = \{[t_{e_1,k-1}^l \dots t_{e_n,k-1}^l]'\}_{e_1,\dots,e_n}$ and the total number of $\mathbf{\Psi}_{k-1,t}$ is $\tau_1 \times \dots \times \tau_n$. Then, using the prior sampled-knots, one can predict the sample knots $\mathbf{\Psi}_{k,t}$ as

$$\mathbf{\Psi}_{k,t}^{e_1,\dots,e_n} \quad = \quad f_{k,\mathbf{M}_k}(\mathbf{\Psi}_{k-1,t}^{e_1,\dots,e_n}, 0, \mathbf{M}_k = \mathfrak{q}) \tag{50}$$

where the $f_{k,\mathbf{M}_k}(\cdot,\cdot,\cdot)$ is the mode-dependent function of transition in (3). Next, the predicted knots in each dimension are selected by projecting all sample vectors $\mathbf{\Psi}_{k,t}^{e_1,\dots,e_n}$ into the axis of the respective dimension (l-th dimension) with possibly $\tau_1 \times \cdots \times \tau_n$ overlapping points in each axis for the n-dimensional problem. The l-th dimensional predicted knots are sorted in a non-decreasing order denoted as

$$\{t_{1',k}^l, t_{2',k}^l, \dots, t_{(\tau_1 \times \dots \times \tau_n)',k}^l\} \tag{51}$$

Using (49) and known prior number of targets and their states, interactively shaped B-spline curve's l-th knot vector can be written as

$$\mathbf{t}_{k-1}^{l} = \{t_{1,k-1}^{l}, \ldots, t_{\zeta_{h_{k-1}},k-1}^{l}, \ldots, t_{\tau,k-1}^{l}\} \tag{52}$$

where $h_{k-1} \in 1, 2, \cdots, \vartheta_{k-1}$. The elements of knot vector $\mathbf{t}_{k-1}^{l}$ are in non-decreasing order and (52) can be written for n dimensional knot $\mathbf{t}_{k-1} = \{\mathbf{t}_{k-1}^{1}, \ldots, \mathbf{t}_{k-1}^{n}\}$. Next, extract ϑ_{k-1} target states as

$$\mathfrak{x}_{l,k-1} \quad = \quad \mathfrak{x}_{h_{k-1},k-1} = [t_{\zeta_{h_{k-1}},k-1}^{1}, \ldots, t_{\zeta_{h_{k-1}},k-1}^{n}] \tag{53}$$

where $l = h_{k-1} \in (1, 2, \cdots, \vartheta_{k-1})$ and the predicted states of the targets at time k as

$$\mathfrak{x}_{l,k} \quad = \quad f_{k,\mathbf{M}_k}(\mathfrak{x}_{l,k-1}, 0, \mathbf{M}_k) \qquad l \in 1, 2, \ldots, \vartheta_{k-1} \tag{54}$$

Then, using (51) one can select the knots. The first and the last predicted knots are selected as $t_{1,k}^{l} = t_{1',k}^{l}$ and $t_{\tau_l,k}^{l} = t_{(\tau_1 \times \ldots \times \tau_n)',k}^{l}$, respectively. The rest of the knots can be selected close to the l-th dimensional predicted states $\mathfrak{x}_{l,k}$, where $l \in 1, 2, \ldots, \vartheta_{k-1}$. Knot removal can be invoked to remove unnecessary knots, but the first and the last knot elements are never removed. This method can be applied for all dimensions and the use of this technique for determining knots guarantees that the spline covers the area where the PHD of system state is substantial. The mode-dependent coefficients of the spline transition density $\mathbb{P}_{j_1,\ldots,j_{2n}}$ can be determined as described in [24].

The mode-dependent spline predicted density can be calculated using (15) as

$$\begin{aligned} \mathbf{B}_{k|k-1}(\mathbf{x}_k, \mathbf{M}_k = \mathfrak{q}) \quad = \quad & \mathbf{B}_{\mathbf{c},k|k-1}(\mathbf{x}_k, \mathbf{M}_k = \mathfrak{q}) \\ & + \mathbf{B}_{\mathbf{s},k|k-1}(X_k, \mathbf{M}_k = \mathfrak{q}) \\ & + \mathbf{B}_{\mathbf{nb},k}(\mathbf{x}_k, \mathbf{M}_k = \mathfrak{q}) \end{aligned} \tag{55}$$

The predicted MM-SPHD for the existing targets can be determined as [20]

$$\begin{aligned} D_{\mathbf{c},k|k-1}(\mathbf{x}_k, \mathbf{M}_k = \mathfrak{q}) \quad = \quad & \int P_{\mathfrak{s},k|k-1}(\mathbf{x}_{k-1}, \mathbf{M}_k = \mathfrak{q}) \\ & \cdot p_{k|k-1}(\mathbf{x}_k, \mathbf{M}_k = \mathfrak{q} | \mathbf{x}_{k-1}, \mathbf{M}_{k-1} = \mathfrak{p}) \\ & \cdot \tilde{D}_{k|k-1}(\mathbf{x}_{k-1}, \mathbf{M}_k = \mathfrak{q} | Z^{(k-1)}) \\ & \cdot d\mathbf{x}_{k-1} \end{aligned} \tag{56}$$

and the spline predicted MM-SPHD for the existing targets as

$$\begin{aligned}
\mathbf{B}_{\mathbf{c},k|k-1}(\mathbf{x}_k,\mathbf{M}_k=\mathfrak{q}) &= \int P_{\mathfrak{s},k|k-1}(\mathbf{x}_{k-1},\mathbf{M}_k=\mathfrak{q})\sum_{j_1}^{n_s}\cdots\sum_{j_{2n}}^{n_s}\mathbb{P}_{j_1,\ldots,j_{2n}} \\
&\quad\cdot B_{j_1,p,\mathbf{t}_k^1}(\mathbf{x}_k^1,\mathbf{M}_k=\mathfrak{q})\ldots B_{j_n,p,\mathbf{t}_k^n}(\mathbf{x}_k^n,\mathbf{M}_k=\mathfrak{q}) \\
&\quad\cdot B_{j_{n+1},p,\mathbf{t}_{k-1}^1}(\mathbf{x}_{k-1}^1,\mathbf{M}_{k-1}=\mathfrak{p})\ldots \\
&\quad\cdot B_{j_{2n},p,\mathbf{t}_{k-1}^n}(\mathbf{x}_{k-1}^n,\mathbf{M}_{k-1}=\mathfrak{p})\sum_{i_1}^{n_s}\cdots\sum_{i_n}^{n_s}\mathbb{P}_{i_1,\ldots,i_n} \\
&\quad\cdot B_{i_1,p,\mathbf{t}_{k-1}^1}(\mathbf{x}_{k-1}^1,\mathbf{M}_k=\mathfrak{q})\ldots \\
&\quad\cdot B_{i_n,p,\mathbf{t}_{k-1}^n}(\mathbf{x}_{k-1}^n,\mathbf{M}_k=\mathfrak{q})\ d\mathbf{x}_{k-1}^1\ldots d\mathbf{x}_{k-1}^n \\
&= \sum_{j_1}^{n_s}\cdots\sum_{j_{2n}}^{n_s}\mathbb{P}_{j_1,\ldots,j_{2n}}B_{j_1,p,\mathbf{t}_k^1}(\mathbf{x}_k^1,\mathbf{M}_k=\mathfrak{q})\ldots \\
&\quad\cdot B_{j_n,p,\mathbf{t}_k^n}(\mathbf{x}_k^n,\mathbf{M}_k=\mathfrak{q})\sum_{i_1}^{n_s}\cdots\sum_{i_n}^{n_s}\mathbb{P}_{i_1,\ldots,i_n} \\
&\quad\cdot\int P_{\mathfrak{s},k|k-1}(\mathbf{x}_{k-1},\mathbf{M}_k=\mathfrak{q}) \\
&\quad\cdot B_{j_{n+1},p,\mathbf{t}_{k-1}^1}(\mathbf{x}_{k-1}^1,\mathbf{M}_{k-1}=\mathfrak{p})\ldots \\
&\quad\cdot B_{j_{2n},p,\mathbf{t}_{k-1}^n}(\mathbf{x}_{k-1}^n,\mathbf{M}_{k-1}=\mathfrak{p}) \\
&\quad\cdot B_{i_1,p,\mathbf{t}_{k-1}^1}(\mathbf{x}_{k-1}^1,\mathbf{M}_k=\mathfrak{q})\ldots \\
&\quad\cdot B_{i_n,p,\mathbf{t}_{k-1}^n}(\mathbf{x}_{k-1}^n,\mathbf{M}_k=\mathfrak{q}) \\
&\quad\cdot d\mathbf{x}_{k-1}^1\ldots d\mathbf{x}_{k-1}^n
\end{aligned} \tag{57}$$

Note that the order of summation and integration of splines is exchangeable [4]. Define two $2n$-dimensional matrices Υ and $\hbar$, and one n-dimensional matrix $\wp$ as follows:

$$\begin{aligned}
\Upsilon_{j_{n+1},\ldots,j_{2n},i_1,\ldots,i_n} &= \int P_{\mathfrak{s},k|k-1}(\mathbf{x}_{k-1},\mathbf{M}_k=\mathfrak{q}) \\
&\quad\cdot B_{j_{n+1},p,\mathbf{t}_{k-1}^1}(\mathbf{x}_{k-1}^1,\mathbf{M}_{k-1}=\mathfrak{p})\ldots \\
&\quad\cdot B_{j_{2n},p,\mathbf{t}_{k-1}^n}(\mathbf{x}_{k-1}^n,\mathbf{M}_{k-1}=\mathfrak{p}) \\
&\quad\cdot B_{i_1,p,\mathbf{t}_{k-1}^1}(\mathbf{x}_{k-1}^1,\mathbf{M}_k=\mathfrak{q})\ldots \\
&\quad\cdot B_{i_n,p,\mathbf{t}_{k-1}^n}(\mathbf{x}_{k-1}^n,\mathbf{M}_k=\mathfrak{q}) \\
&\quad\cdot d\mathbf{x}_{k-1}^1\ldots d\mathbf{x}_{k-1}^n
\end{aligned} \tag{58}$$

Let $\hbar_{\mathfrak{j}}=\mathbb{P}_{\mathfrak{j}}$ and $\wp_{\mathfrak{i}}=\mathbb{P}_{\mathfrak{i}}$. Using (56), (58) and (60) with additional manipulations, it can be shown that

$$\begin{aligned}
\mathbf{B}_{\mathbf{c},k|k-1}(\mathbf{x}_k,\mathbf{M}_k=\mathfrak{q}) &= \sum_{j_1}\cdots\sum_{j_n}\mathbb{P}_{j_1,\ldots,j_n} \\
&\quad\cdot B_{j_1,p,\mathbf{t}_k^1}(\mathbf{x}_k^1,\mathbf{M}_k=\mathfrak{q})\ldots \\
&\quad\cdot B_{j_n,p,\mathbf{t}_k^n}(\mathbf{x}_k^n,\mathbf{M}_k=\mathfrak{q})
\end{aligned} \tag{59}$$

where $\mathbb{P}_{j_1,\ldots,j_n}$ is given by

$$\mathbb{P}_{j_1,\ldots,j_n} = \sum_{i_1}\cdots\sum_{i_n}\wp_{i_1,\ldots,i_n}\sum_{j_{n+1}}\cdots\sum_{j_{2n}}\hbar_{j_1,\ldots,j_{2n}}\Upsilon_{j_{n+1},\ldots,j_{2n},i_1,\ldots,i_n} \tag{60}$$

where $\mathbf{B}_{\mathbf{c},k|k-1}(\mathbf{x}_k, \mathbf{M}_k = \mathfrak{q})$ denotes the $\mathfrak{q}$-th mode-dependent existing targets' predicted SPHD.

A similar approach as described for $\mathbf{B}_{\mathbf{c},k|k-1}(\mathbf{x}_k, \mathbf{M}_k = \mathfrak{q})$ can be applied to determine the mode-dependent spawned targets' predicted SPHD $\mathbf{B}_{\mathbf{s},k|k-1}(\mathbf{x}_k, \mathbf{M}_k = \mathfrak{q})$. The mode-dependent SPHD of new targets $\mathbf{B}_{\mathbf{nb},k}(\mathbf{x}_k, \mathbf{M}_k = \mathfrak{q})$ can be determined as follows [24]:

First, the mode-dependent posterior probability for an observed measurement that originates from a new target $P_k(\Im_i, \mathbf{M}_k = \mathfrak{q})$ is determined as

$$P_k(\Im_i, \mathbf{M}_k = \mathfrak{q}) \quad = \quad \frac{\mathbf{B}_{\Im,k}(\mathbf{z}_i, \mathbf{M}_k = \mathfrak{q})}{\mathbf{B}_{\lambda,k}(\mathbf{z}_i) + \sum_{\mathfrak{q}=1}^{\mathfrak{r}} \mathbf{B}_{\Im,k}(\mathbf{z}_i, \mathbf{M}_k = \mathfrak{q})}\,, \tag{61}$$

where $\mathbf{z}_i \in Z_k$, $i = 1, \ldots, \beth_k$ and

$$\begin{aligned} \mathbf{B}_{\Im,k}(\mathbf{z}_i, \mathbf{M}_k = \mathfrak{q}) \quad = \quad & \int P_{\mathfrak{d},k}(\mathbf{x}_k, \mathbf{M}_k = \mathfrak{q}) \\ & \cdot \mathbf{B}_{l,k}(\mathbf{z}_i | \mathbf{x}_k, \mathbf{M}_k = \mathfrak{q}) \\ & \cdot \mathbf{B}_{k|k-1}(\mathbf{x}_k, \mathbf{M}_k = \mathfrak{q}) \\ & \cdot d\mathbf{x}_k \end{aligned} \tag{62}$$

where $\Im_i$ and $\beth_k$ denote the i-th observed measurement from a new target and the total number of measurements at time k, respectively.

In the above, $\mathbf{B}_{k|k-1}(\mathbf{x}_k, \mathbf{M}_k = \mathfrak{q}) \approx \mathbf{B}_{\mathbf{c},k|k-1}(\cdot) + \mathbf{B}_{\mathbf{s},k|k-1}(\cdot)$ and the spline likelihood density $\mathbf{B}_{l,k}(\cdot)$ can be determined using the measurement model in (5). The spline uniform clutter density is denoted by $\mathbf{B}_{\lambda,k}(\cdot)$ and $P_{\mathfrak{d},k}(\mathbf{x}_k, \mathbf{M}_k = \mathfrak{q})$ denotes the mode-dependent probability of detection.

For each measurement, the mode-dependent posterior probability for it to have originated from a new target is calculated and it is compared with a fine-tuning threshold probability ϵ. That is,

$$N_{\mathbf{nb},i} = \begin{cases} 1 & \text{if } \; P_k(\Im_i, \mathbf{M}_k = \mathfrak{q}) \leqslant \epsilon, \\ 0 & \text{otherwise.} \end{cases} \tag{63}$$

If the number of newborn targets $N_{\mathbf{nb},i}$ is 1, then a newborn target SPHD can be included for measurement i as

$$\mathbf{B}_{\mathbf{nb},k}(\mathbf{x}_k, \mathbf{M}_k = \mathfrak{q}) \quad = \quad \sum_{i=1}^{N_{\mathbf{nb}}} \mathbf{B}_{\mathbf{nb},k,i}(\mathbf{z}_i) \tag{64}$$

where $\mathbf{B}_{\mathbf{nb},k,i}$ is the SPHD of a newborn target with mean $\mathbf{z}_i$ and variance of measurement noise. The total number of newborn targets per scan is denoted by $N_{\mathbf{nb}}$ and $\mathbf{B}_{\mathbf{nb},k}(\mathbf{x}_k, \mathbf{M}_k = \mathfrak{q})$ denotes the cumulative sum of all the SPHD values of newborn targets at scan k. Overall, if for the i-th measurement, $\mathbf{z}_i$, $P_k(\Im_i, \mathbf{M}_k = \mathfrak{q}) = 1$ then each element of $\mathbf{z}_i$ can be considered as the mean of a newborn target state in its respective dimension with the variance of measurement noise. A newborn target can be added using Gaussian distribution with corresponding mean and variance from each state element of that newborn target. The mode-dependent MM-SPHD of newborn targets, $\mathbf{B}_{\mathbf{nb},k}(\mathbf{x}_k, \mathbf{M}_k = \mathfrak{q})$, depends on system model $\mathfrak{q}$. The expected number of targets can be determined by finding the area of mode-dependent MM-SPHD $\mathbf{B}_{k|k-1}(\mathbf{x}_k, \mathbf{M}_k = \mathfrak{q})$.

C. MM-SPHD update

Note that the MM-SPHD filter provides the PHD estimates in a continuous space in the kinematic state. These predicted MM-SPHD $\mathbf{B}_{k|k-1}(\cdot)$ at any point over the interval $[t_{1,k}, t_{\tau,k}]$ can be determined using (55). Then, the interval where $\mathbf{B}_{k|k-1}(\cdot)$

is substantial can be determined and the value for the likelihood density function $\mathbf{B}_{l,k}(\mathbf{z}_k|\mathbf{x}_k, \mathbf{M}_k = \mathfrak{q})$ can be evaluated for the same interval using (5). The updated posterior MM-SPHD can be determined as [20] (for $\mathfrak{q} = 1, \ldots, \mathfrak{r}$)

$$\begin{aligned} D_{k|k}(\mathbf{x}_k, \mathbf{M}_k = \mathfrak{q}|Z^{(k)}) &= (1 - P_{\mathfrak{d},k}(\mathbf{x}_k, \mathbf{M}_k = \mathfrak{q}))\mathbf{B}_{k|k-1}(\mathbf{x}_k, \mathbf{M}_k = \mathfrak{q}) \\ &\quad + \sum_{\mathbf{z_k} \in Z_k} \frac{\mathbf{B}_\phi(\mathbf{x}_k, \mathbf{M}_k = \mathfrak{q})}{\mathbf{B}_\lambda(\mathbf{z_k}) + \int \mathbf{B}_\phi(\mathbf{x}_k, \mathbf{M}_k = \mathfrak{q}) d\mathbf{x}_k} \\ &= \sum_{\iota_1, \ldots, \iota_n} \mathbb{P}_{\iota_1, \ldots, \iota_n} B_{\iota_1, p, \mathbf{t}_k^1}(\mathbf{x}_k^1, \mathbf{M}_k = \mathfrak{q}) \ldots \\ &\quad \cdot B_{\iota_n, p, \mathbf{t}_k^n}(\mathbf{x}_k^n, \mathbf{M}_k = \mathfrak{q}) \end{aligned} \tag{65}$$

where $\mathbf{B}_\phi(\mathbf{x}_k, \mathbf{M}_k = \mathfrak{q})$ can be evaluated as follows:

$$\begin{aligned} \mathbf{B}_\phi(\mathbf{x}_k, \mathbf{M}_k = \mathfrak{q}) &= P_{\mathfrak{d},k}(\mathbf{x}_k, \mathbf{M}_k = \mathfrak{q}) \\ &\quad \cdot \mathbf{B}_{l,k}(\mathbf{x}_k, \mathbf{M}_k = \mathfrak{q}) \\ &\quad \cdot \mathbf{B}_{k|k-1}(\mathbf{x}_k, \mathbf{M}_k = \mathfrak{q}) \end{aligned} \tag{66}$$

Then, the updated MM-SPHD can be further simplified as

$$\begin{aligned} \mathbf{B}_{k|k}(\mathbf{x}_k, \mathbf{M}_k = \mathfrak{q}) &= \sum_{\iota_1, \ldots, \iota_n} \mathbb{P}_{\iota_1, \ldots, \iota_n} \\ &\quad \cdot B_{\iota_1, p, \mathbf{t}_k^1}(\mathbf{x}_k^1, \mathbf{M}_k = \mathfrak{q}) \ldots \\ &\quad \cdot B_{\iota_n, p, \mathbf{t}_k^n}(\mathbf{x}_k^n, \mathbf{M}_k = \mathfrak{q}) \end{aligned} \tag{67}$$

where the set of posterior knots is denoted by $\mathbf{t}_k$. The spline posterior density (67) is only assessed over the range where it is substantial. In this substantial region, the posterior knots are uniformly distributed [24]. The expected number of targets from model $\mathfrak{q}$ can be determined by taking the integral of mode-dependent MM-SPHD updated equation $\mathbf{B}_{k|k}(\mathbf{x}_k, \mathbf{M}_k = \mathfrak{q})$ as

$$\hat{N}_{k|k}^{\mathfrak{q}} = \int_{\mathcal{E}_s} \mathbf{B}_{k|k}(\mathbf{x}_k, \mathbf{M}_k = \mathfrak{q}) d\mathbf{x}_k \tag{68}$$

The total number of targets can be determined as

$$\hat{N}_{k|k} = \sum_{\mathfrak{q}=1}^{\mathfrak{r}} \hat{N}_{k|k}^{\mathfrak{q}} \tag{69}$$

Mode probability can be updated by first integrating a particular model's mode-dependent updated MM-SPHD. Then the result should be divided by the total expected/average number of targets [20].

VI. Simulation Results

In this section, a nonlinear maneuvering multitarget tracking example is presented to validate the performance of the proposed MM-SPHD filter. The selected example is a multidimensional one dealing with the bearing-only ground target tracking problem, which arises in many practical applications such as submarine tracking or airborne surveillance using a passive radar [24]. Note that a standard radar tracking problem, where the range and azimuth measurements are available for tracking can be converted into a linear problem. Also, the bearing only tracking problem is inherently ill-conditioned [16, 27] and is better suited for comparing nonlinear target tracking algorithms.

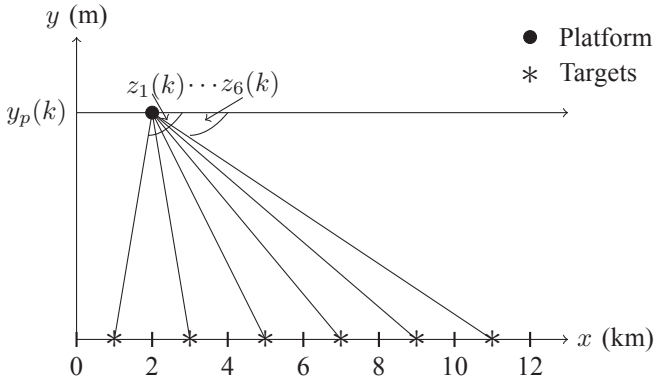

Fig. 3. Motion of the platform and the six targets

As shown in Figure 3, the sensor is on an aircraft with

$$x_p(k) = \bar{x}_p(k) + \Delta x_p(k) \qquad k = 0, 1, \ldots, 40 \tag{70}$$

$$y_p(k) = \bar{y}_p(k) + \Delta y_p(k) \qquad k = 0, 1, \ldots, 40 \tag{71}$$

where $x_p(k)$ and $y_p(k)$ are the x and y positions of the platform, respectively. The average platform position coordinates are denoted by $\bar{x}_p(k)$ and $\bar{y}_p(k)$, k is the time index and the perturbations $\Delta x_p(k)$ and $\Delta y_p(k)$ are assumed to be mutually independent zero-mean Gaussian white noise sequences with variances $\sigma^2_{\Delta x_p} = 1$ and $\sigma^2_{\Delta y_p} = 1$, respectively. Note that this problem has been used to compare nonlinear filtering tracking algorithms before [2, 10, 24]. The average unperturbed platform motion is assumed to be horizontal with a constant velocity. Its coordinates are given by

$$\bar{x}_p(k) = 100k * T \quad \text{(m)} \tag{72}$$

$$\bar{y}_p(k) = 10000 \quad \text{(m)} \tag{73}$$

where the sampling time $T = 10$s. A system with three models is considered here to demonstrate the MM-SPHD. In the second and third models, a time-varying control term is added. The three system models are

$$\mathbf{x}_i^1(k) = \begin{bmatrix} 1 & T \\ 0 & 1 \end{bmatrix} \mathbf{x}_i^1(k-1) + \begin{bmatrix} T^2/2 \\ T \end{bmatrix} \nu_{1,k-1}, \tag{74}$$

$$\mathbf{x}_i^2(k) = \begin{bmatrix} 1 & T \\ 0 & 1 \end{bmatrix} \mathbf{x}_i^2(k-1) + \begin{bmatrix} -T/2 \\ -T/500 \end{bmatrix} (k-1) + \begin{bmatrix} T^2/2 \\ T \end{bmatrix} \nu_{2,k-1} \tag{75}$$

and

$$\mathbf{x}_i^3(k) = \begin{bmatrix} 1 & T \\ 0 & 1 \end{bmatrix} \mathbf{x}_i^3(k-1) + \begin{bmatrix} T/2 \\ T/500 \end{bmatrix} (k-1) + \begin{bmatrix} T^2/2 \\ T \end{bmatrix} \nu_{3,k-1} \tag{76}$$

where the target state is

$$\mathbf{x}_i(k) = \begin{bmatrix} x_i^1(k) \\ x_i^2(k) \end{bmatrix} \quad i = 1, 2, 3, 4, 5, 6 \tag{77}$$

and x_i^1 denotes the position in meters while x_i^2 denotes the velocity in m/s of the i-th target and $\nu_{1,k}$, $\nu_{2,k}$, and $\nu_{3,k}$ are all zero-mean white Gaussian random variables with standard deviation $\sigma_{\nu_{1,k}} = 0.05$ m/s^2, $\sigma_{\nu_{2,k}} = 0.08$ m/s^2 and $\sigma_{\nu_{3,k}} = 0.07$ m/s^2, respectively.

In this example, six maneuvering targets are traveling with initial states

$$[\mathbf{x}_1(k)\ \mathbf{x}_2(k)\ \mathbf{x}_3(k)\ \mathbf{x}_4(k)\ \mathbf{x}_5(k)\ \mathbf{x}_6(k)] = \begin{bmatrix} 1000 & -1000 & 17000 & -17000 & 10000 & -10000 \\ 40 & -40 & -50 & 50 & 50 & -50 \end{bmatrix} \tag{78}$$

and the start and end times of the six targets are (1,40), (1,40), (16,38), (16,38), (3,33) and (3,33), respectively.

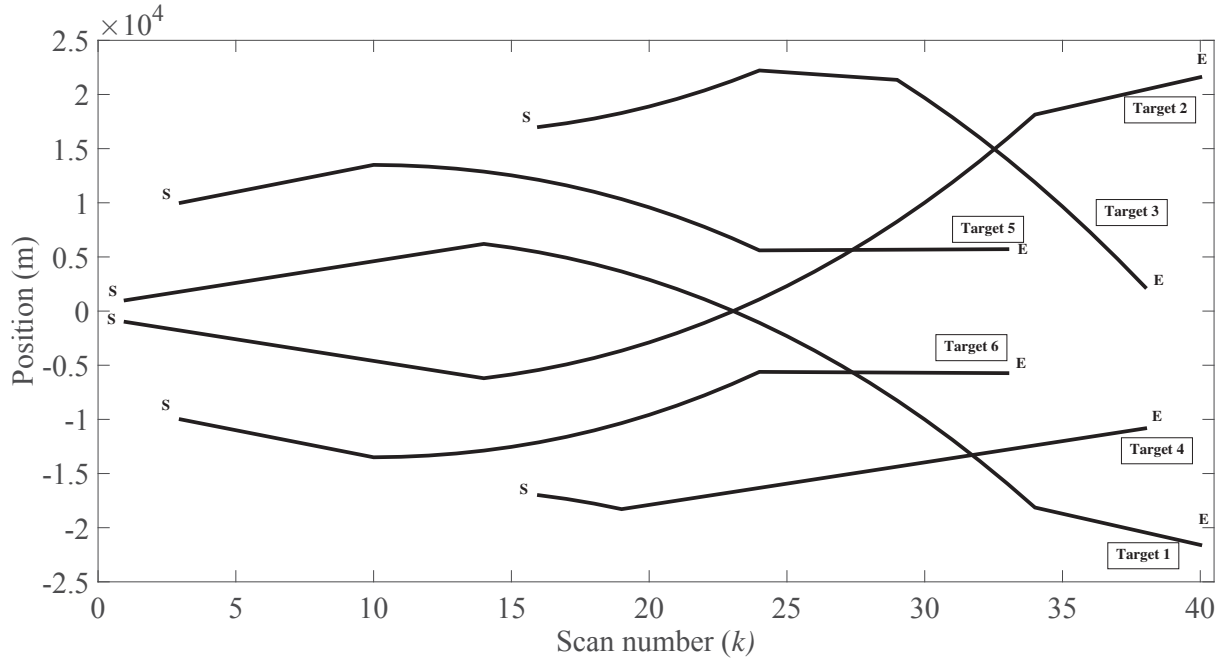

Fig. 4. True target trajectories.

As shown in Figure 4, Target 1 moves for the first 140s at a almost steady velocity with an early velocity of 40 m/s, then moves in a positive direction for the next 190s and, finally moves at a almost steady velocity for the last 60s. Target 2 moves for the first 140s at a almost steady velocity with an early velocity of -40 m/s, then moves in the negative direction for 190s and, finally moves at a almost steady velocity for the last 60s. Target 3 moves 90s in the negative direction with an early velocity of -50 m/s, then moves at a almost steady velocity for 50s and for the last 90s moves in a positive direction. Target 4 moves 40s in the positive direction with an early velocity of 50 m/s, then moves at a almost steady velocity for last 180s. Target 5 moves for the first 70s at a almost steady velocity with an early velocity of 50 m/s, then moves in a positive direction for the next 140s and, finally moves at a almost steady velocity for the last 90s. Target 6 moves for the first 70s at a almost steady velocity with an early velocity of -50 m/s, then moves in the negative direction for 140s and, finally moves at a almost steady velocity for the last 90s.

Targets move along the X-axis and these six targets, which have a probability of survival $P_{\mathtt{s},k} = 0.98$, appear and disappear at specific times. The Markovian model transition probability matrices π_{pq} for the six targets are

$$\pi_{pq} = \begin{bmatrix} 1/3 & 1/3 & 1/3 \\ 2/5 & 3/5 & 0.0 \\ 2/5 & 0.0 & 3/5 \end{bmatrix}, \tag{79}$$

and the initial model probabilities for the models are 0.33.

Each target is detected with probability $P_{\mathfrak{d},k} = 0.95$ and the target-originated measurements follow the observation model

$$z_i(k) \quad = \quad h[x_p(k), y_p(k), x_i^1(k)] + \omega(k) \qquad i = 1, 2, 3, 4, 5, 6 \tag{80}$$

where

$$h[.] \quad = \quad \tan^{-1} \frac{y_p(k)}{x_i^1(k) - x_p(k)} \qquad i = 1, 2, 3, 4, 5, 6 \tag{81}$$

is the angle between the X-axis and the line of sight from the sensor to the targets. The sensor noise $\omega(k)$ is zero-mean white Gaussian with $\sigma_\omega = 2^\circ$. The sensor noise is assumed independent of the sensor platform perturbations. The received measurements include false alarms. The sensor's two dimensional resolution cell has area $A = \left(3\sqrt{2.3}\right)^2 \approx 20$. The return signal is processed by a quadrature receiver with a Constant False Alarm Rate (CFAR) setting for varying P_{fa} per cell, which yields a false alarm spatial density of $\lambda = P_{fa}/A$ (degree)$^{-1}$. Note, initially the signal to noise ratio (SNR) in a cell is taken as 5 dB and as in [11], but keeping the SNR constant and for varying (preselected) P_d the detection threshold values were determined. Using the detection threshold values the P_{fa} values were determined. The clutter is modeled as uniformly distributed in the measurement space with average false alarm rate λ over the whole surveillance region $[0, \pi]$ rad [11].

For tracking multiple targets, an MM-SPHD filter of order 3 is used with 20 knots for position and 10 knots for velocity. At scan $k = 0$, all measurements are used to initialize newborn targets as described in Section V-B. The probability of target spawning is assumed to be zero and the probability of spontaneous target birth is 0.01.

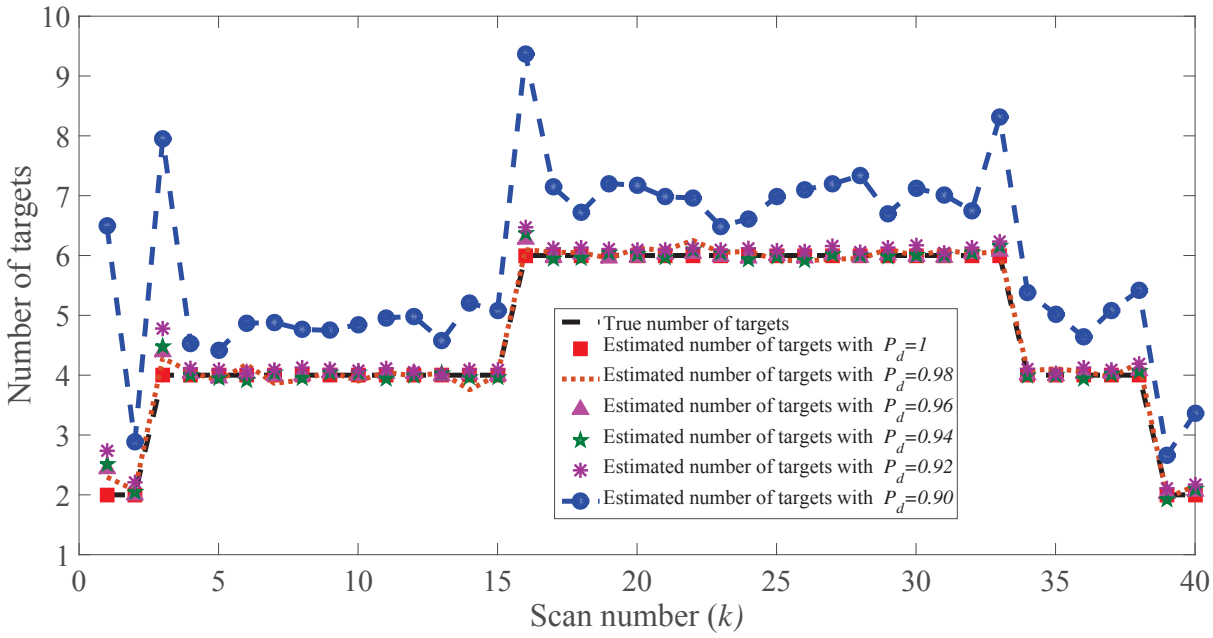

Fig. 5. True vs. average of estimated number of targets from 1000 runs ($\sigma_\omega = 2^\circ$).

As shown in Figure 5, the MM-SPHD filter accurately estimates the number of targets in five different scenarios out of six. In general, the performance of the PHD filter degrades in low probability of detection scenarios [14]. As illustrated in Figure 5, decrease in P_d affects the stability of the MM-SPHD filter. This can be alleviated using an averaging window method as in [14]. However, for real-time target tracking with very low SNR (dim targets) this method is not viable and, as shown in

Figure 5, scenarios with probability of detection smaller than 0.92 yield poor performance in terms of cardinality estimates. In Figure 5, P_d denotes the probability of detection.

The standard PHD filter does not have a closed-form solution and cannot estimate target states directly. Target states can be extracted using K-means clustering algorithm [28] or Expectation-Maximization (EM) based peak extraction approach [29]. The MM-SPHD typically includes many local maxima, which may or may not correspond to various targets of cardinality $\hat{N}_{k|k}$. At scan k, the false-alarm generated peaks in the MM-SPHD are removed by thresholding the spline coefficients. The state estimates can be determined by finding the knot elements with a high MM-SPHD in each dimension and this process has to be done for all $\hat{N}_{k|k}$ targets. Another way is to identify the local maxima in the MM-SPHD surface numerically through a local search.

The targets are associated to tracks using global nearest-neighbor assignment [18] depending on the mean of each target-cluster. As shown in Figure 6, all six targets appear and disappear at various times during the surveillance interval. Also shown in Figure 6 are the averages of the estimated trajectories by using Monte Carlo trials and averaging the values over those trials.

As shown in Figure 7, the MM-SPHD filter estimated the velocities of all targets accurately. The mean velocity of newborn targets is selected randomly from a uniform distribution in the interval $[-100, 100]$ m/s and the standard deviation is assumed to be 0.4 m/s. Knots are dynamically moved along the tracks using an optimal knot selection process to add or delete more knots to better capture the MM-SPHD. This technique is used to alleviate track ID switches.

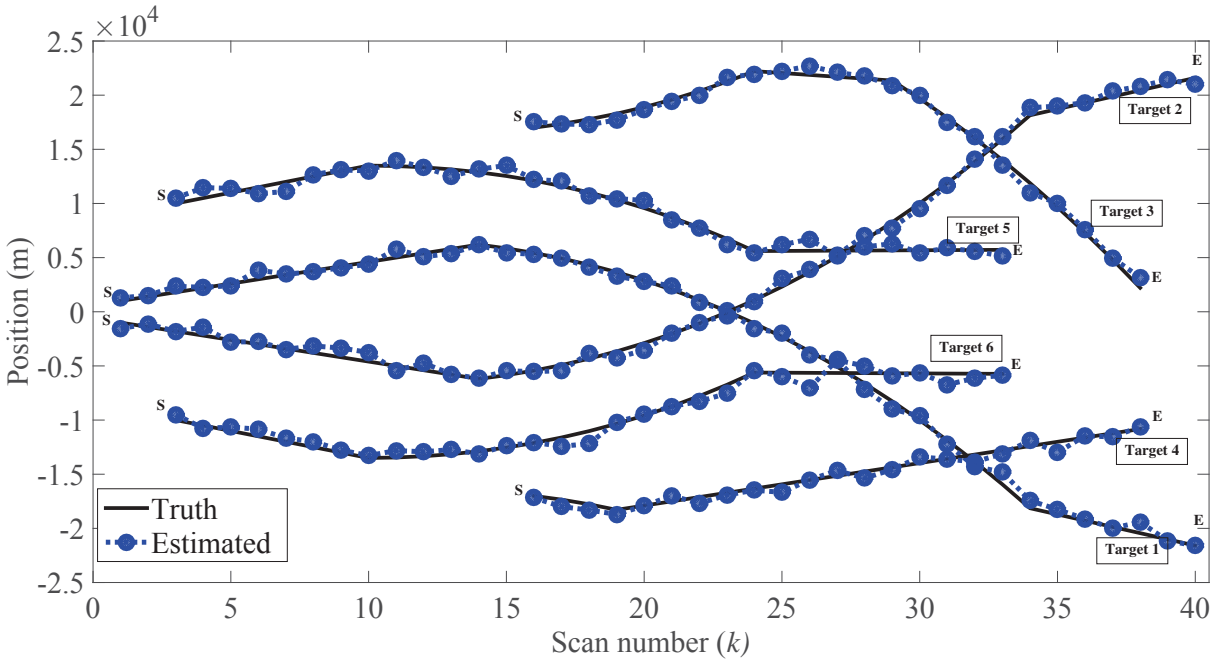

Fig. 6. True position vs. average of estimated positions from 1000 runs ($\sigma_\omega = 2°$, **S**: start, **E**: end).

Table I shows that the choice of knots has significant influence on the performance of the MM-SPHD filter. The selection of the number of knots depends on the application, especially on target separation. Increasing the number of knots affects the complexity of the MM-SPHD filter, but results in better performance in terms of position RMSE. Note that with optimal knot selection, the MM-SPHD filter performance can be improved but with higher complexity.

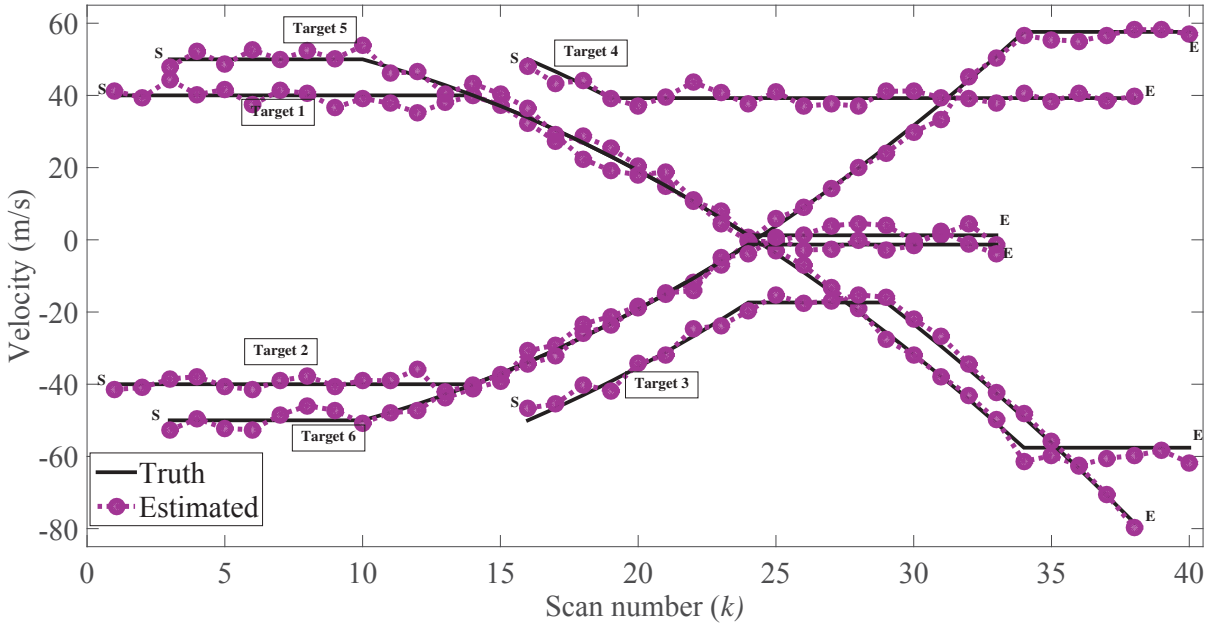

Fig. 7. True velocity vs. average of estimated velocities from 1000 runs ($\sigma_\omega = 2°$, **S**: start, **E**: end).

TABLE I

AVERAGE PERFORMANCE FROM 1000 RUNS VS. NUMBER OF KNOTS ($\sigma_\omega = 2°$, NUMBER OF TARGETS (FIXED) = 6, n_{Pk}: NUMBER OF POSITION KNOTS, n_{Vk}: NUMBER OF VELOCITY KNOTS)

Number of Knots	RMSE (m)	CPU Time (s)
$n_{Pk} = 10$, $n_{Vk} = 5$	694.05	5.7
$n_{Pk} = 20$, $n_{Vk} = 10$	440.02	7.8
$n_{Pk} = 40$, $n_{Vk} = 18$	385.58	10.190
$n_{Pk} = 50$, $n_{Vk} = 20$	360.87	13.475
$n_{Pk} = 60$, $n_{Vk} = 22$	359.10	15.190
$n_{Pk} = 70$, $n_{Vk} = 25$	358.59	16.090

Next, the original example is analyzed further with an increasing number of targets, but with fixed values for the number of position knots $n_{Pk} = 20$ and the number of velocity knots $n_{Vk} = 10$. As shown in Table II, increasing the number of targets for a given number of knots adversely affects the performance of the MM-SPHD filter in terms of RMSE (averaged over all the targets and Monte Carlo runs) and computational time.

The normalized estimation error squared (NEES) [2] and optimal sub-pattern assignment (OSPA) [26] are used as performance metrics for the example.

The OSPA [26] metric measures the miss-distance between a set of true targets and a set of estimated tracks as a combination of localization error and cardinality error [9]. Let $X = \{x_1, \cdots, x_{\acute{n}}\}$ and $Y = \{y_1, \cdots, y_{\acute{m}}\}$ be two finite sets. Here, X denotes

TABLE II

AVERAGE PERFORMANCE FROM 1000 RUNS VS. NUMBER OF TARGETS ($\sigma_\omega = 2^\circ$, $n_{Pk} = 20$, $n_{Vk} = 10$, FIXED NUMBER OF KNOTS)

Number of Targets	RMSE (m)	CPU Time (s)
5	345	7.775
10	465	8.500
15	639	9.125
20	1225	9.750
40	2253	10.650

true finite set of targets and Y denotes the estimated finite set of tracks. The OSPA metric is defined as

$$\bar{d}_{\acute{p}}^{(\acute{c})}(X,Y) = \begin{cases} 0 & \text{if } \acute{m} = \acute{n} = 0 \\ \Psi(X,Y) & \text{if } \acute{m} \leq \acute{n}. \\ d^{(\acute{c})}(X,Y) & \text{if } \acute{m} > \acute{n} \end{cases} \tag{82}$$

where

$$\Psi(X,Y) \triangleq \left(\frac{1}{\acute{n}} \left(\min_{\pi \in \Pi_{\acute{n}}} \sum_{i=1}^{\acute{m}} d^{(\acute{c})}(x_i, y_{\pi(i)}) + \acute{c}^{\acute{p}}(\acute{n} - \acute{m}) \right) \right)^{\frac{1}{\acute{p}}}$$

and the base distance between x and y denoted by $d^{\acute{c}}(x,y) = \min(\acute{c}, \|x - y\|)$, $\Pi_{\acute{n}}$ is the set of permutations with length $\acute{m}$ on the set of $\{1, \cdots, \acute{n}\}$ where $\acute{n} = \|X\|$ and $\acute{m} = \|Y\|$. In the simulations $\acute{p} = 10$ and $\acute{c} = 100$.

The MM-SPHD filter performance is evaluated along with those of multiple model based Gaussian Mixture Unscented Sequential Monte Carlo Probability Hypothesis Density (GM-USMC-PHD) [35], the Gaussian Mixture Sequential Monte Carlo Probability Hypothesis Density (GM-SMC-PHD) [21] and the Auxiliary Particle Probability Hypothesis Density (AP-PHD) [3] filters.

In the MM-GM-USMC-PHD filter implementation, the importance sampling function approximated in the form of a Gaussian mixture that is a sum of Gaussian components and the maximum number of Gaussian terms $= 100$. The number of samples per GM component or target is set to 2500. The newborn target initialization, resampling and state extraction follow [35]. Note that the GM-USMC-PHD filter does not need resampling because the GM process management for multitarget state extraction and component deletion enables the algorithm to have the same effect as resampling. The Unscented Information Filter (UIF) is the information form of the unscented Kalman filter (UKF) [2]. The UIF is used to compute the mean and the covariance of the Gaussian components.

The GM implementation of the MM-GM-SMC-PHD filter is with the EKF for filtering, pruning parameters of elimination threshold $T_p = 10^{-5}$, merging threshold $T_m = 4$m and maximum number of Gaussian terms 100. The SMC implementation of the MM-GM-SMC-PHD uses the transition density to sample particles. Particles are initialized around measurements [7] and 2500 particles are used per existing target and 50 particles are used for each newborn target. An estimate of the number of targets is determined by summing up all the weights of the particles. The estimation of the number of targets and their state extraction carried as in [21].

The MM-AP-PHD filter uses 2500 particles per existing target, while the number particles per newborn target is set to 100. The initialization of the newborn targets is driven by the measurements. The current measurements are associated with the highest bidder if the bid is at least equals 0.4. The Auxiliary Importance Sampling (AIS) [3] process starts with the selection of the measurements that are well described by the targets' states extracted from the estimated PHD and this is achieved using the Auction algorithm [3]. The state extraction is determined as in [3].

In order to facilitate a fair comparison, we ran all methods with the same multiple model strategy [20]. All PHD filters are initialized without any prior knowledge. The overall filter accuracy performance metric, the OSPA [26], is computed for each filter over 1000 Monte Carlo runs for measurement noise standard deviation levels σ_ω=2° and σ_ω=4°. The OSPA metric measures the combination of both localization and cardinality errors. The average OSPA values are plotted in Figures 8 and 9.

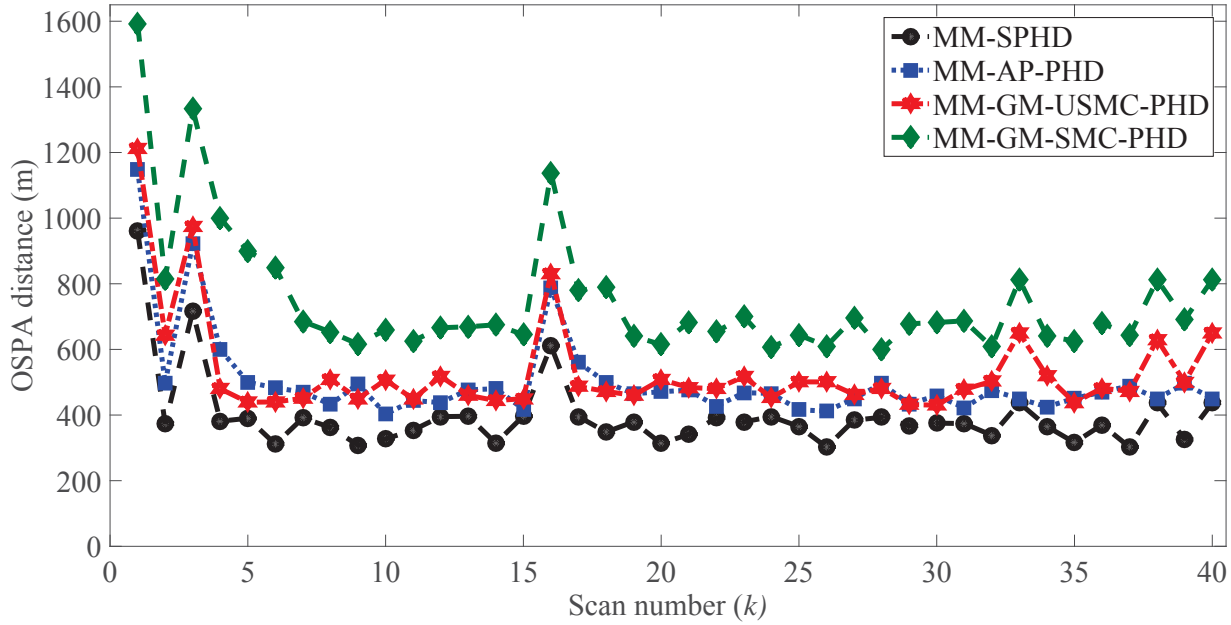

Fig. 8. OSPA distance (m) averaged over 1000 Monte Carlo runs ($\sigma_\omega = 2°$, $\acute{c} = 10$, $\acute{p} = 100$).

The key observation is that the MM-SPHD filter with a few knots performed the best in terms of OSPA for both measurement noise levels. As shown in Figure 8 and 9, high values of OSPA distance occur when new targets are born around time indices $k = 1, 3, 16$. Also targets disappear with small OSPA peaks at time indices $k = 33, 38, 40$. As shown in Figure 9, as the nonlinearity increases with increasing measurement noise levels the GM-based MM-PHD filter perform poorly. Note, missed detections and/or false alarms are handled by taking advantage of dynamic knot movement [24].

Figure 10 reveals the consistency of the MM-SPHD, MM-GM-USMC-PHD, MM-AP-PHD and the MM-GM-SMC-PHD filters in terms of normalized estimation error squared (NEES) compared with the 95% confident-region of the $\mathcal{X}^2$ distributions [2] when the measurement noise standard deviation is $\sigma_\omega = 2°$. Note that the NEES is averaged over all targets and Monte Carlo runs. To illustrate the degeneracy resistance capability of the proposed MM-SPHD filter, the standard deviation of the measurement noise is reduced to σ_ω=0.02°. The model parameters for the filters remain unchanged but with the correct measurement noise level. This scenario causes the particle-based PHD filters to become degenerative. It can be observed

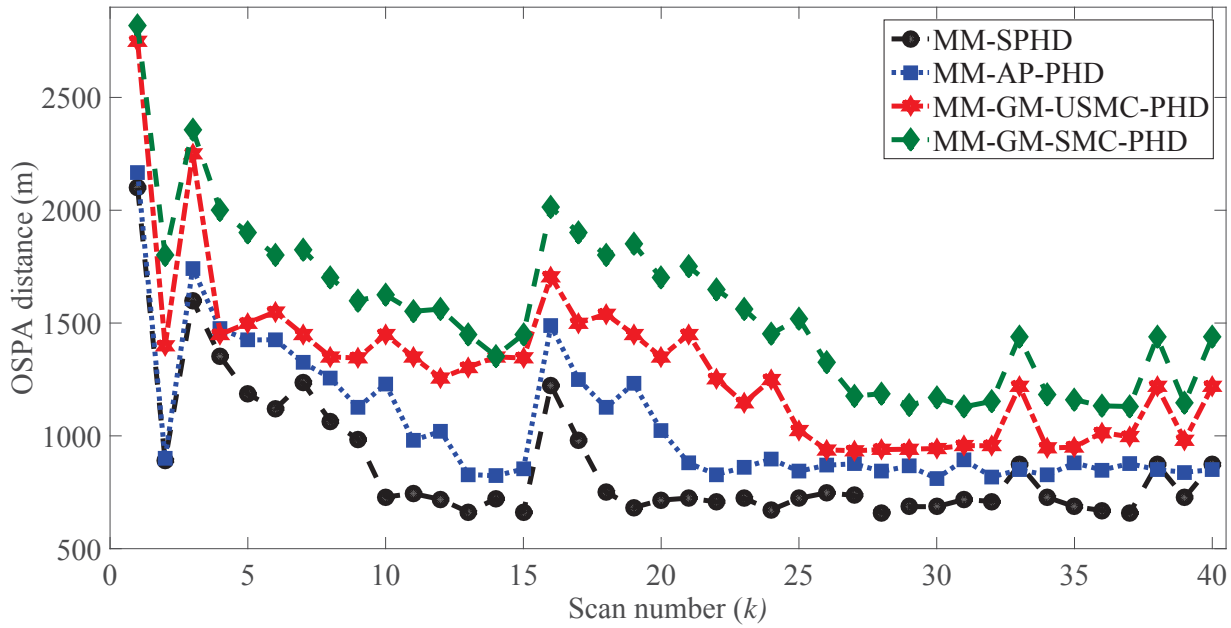

Fig. 9. OSPA distance (m) averaged over 1000 Monte Carlo runs ($\sigma_\omega = 4°$, $\acute{c} = 10$, $\acute{p} = 100$).

from Figure 11 that the MM-SPHD filter is able to provide efficient results with the same 10 velocity knots and 20 position knots. Note that using the Regularized Particle Filter (RPF) [7, 8] can avoid the degeneracy problem caused by sampling and resampling. However, the RPF has the disadvantage is that the samples are no longer guaranteed to asymptotically approximate the posterior [17].

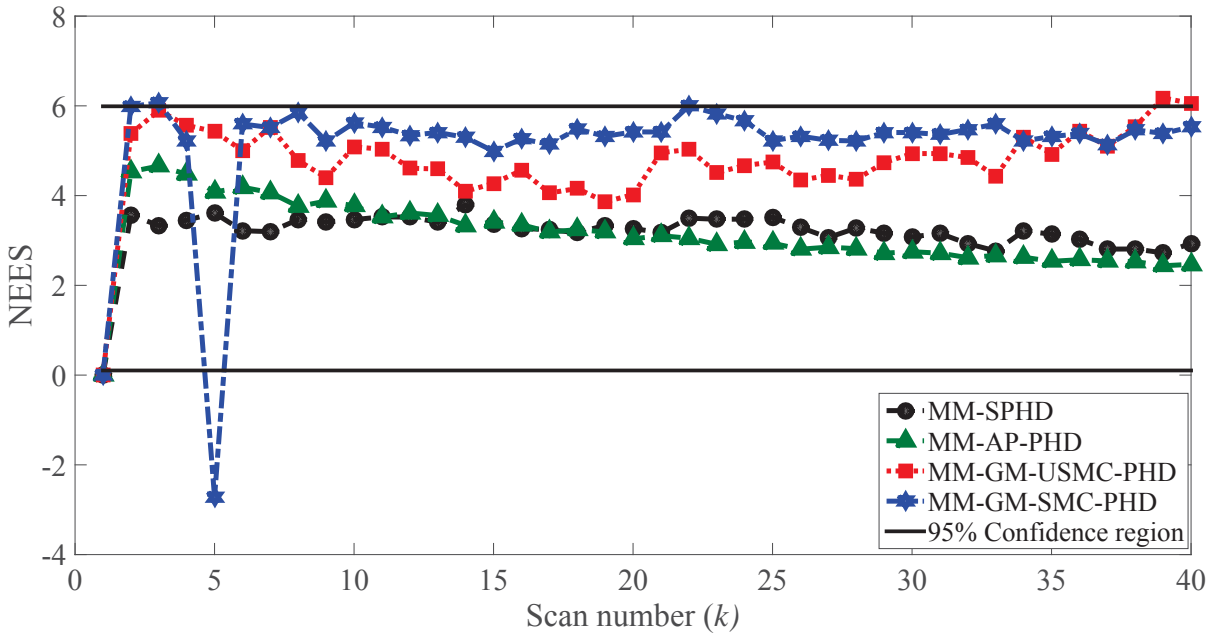

Fig. 10. NEES comparison from 1000 Monte Carlo runs ($\sigma_\omega = 2°$).

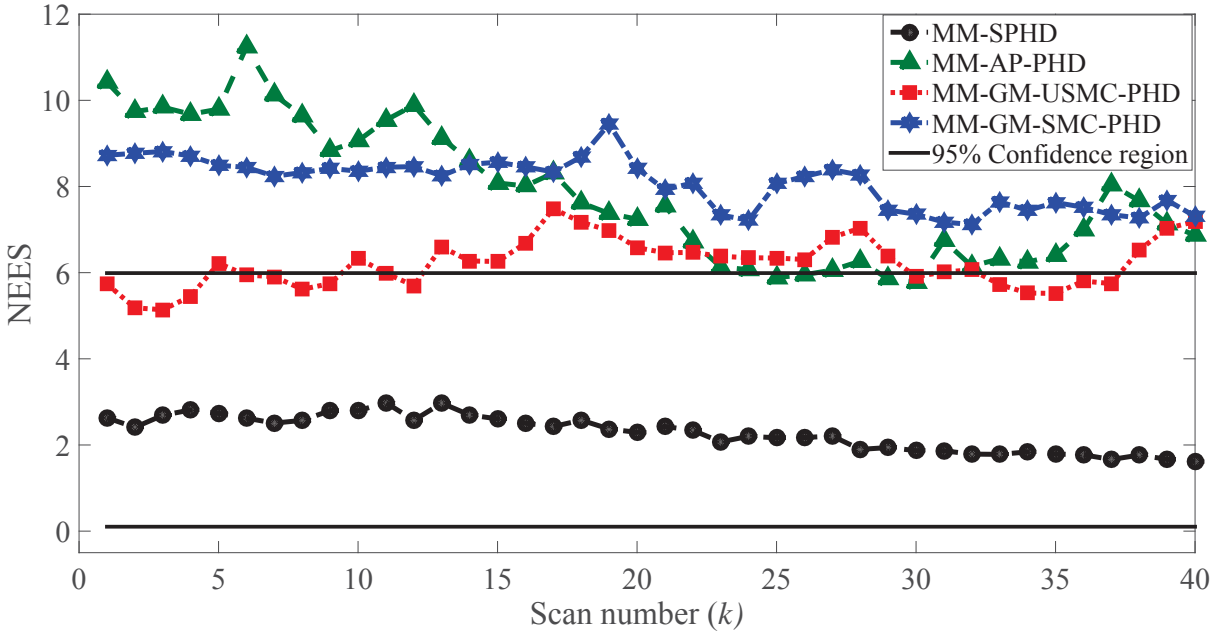

Fig. 11. NEES comparison from 1000 Monte Carlo runs ($\sigma_\omega = 0.02°$).

Further, the performance of the MM-SPHD filter is evaluated against other filters in terms of number of false tracks, track continuity, computational complexity, posterior Cramer-Rao lower bound (PCRLB) and OSPA. As shown in Table III, the average number of false tracks in the MM-SPHD filter is lower than those in other filters. The MM-SPHD filter in Table III used the same method as in [24] to predict knots. In Table III, the new method described in Section V is used. As shown in Table III, both MM-SPHD filters have nearly the same computational complexity. However, in terms of the rest of the metrics, the MM-SPHD filter that used the new method of predicting knots performed better. The MM-SPHD filter with a few knots has the lowest average number of false tracks due to the dynamic movement of its knots, when knots are dynamically (and automatically) moved to ensure that the MM-SPHD filter covers the region where the multimodal posterior SPHD of system state is significant. However, the MM-SPHD filter's performance degrades in high false alarm scenarios, which can be alleviated using a window-averaging method. The multimodal GM-USMC-PHD and GM-SMC-PHD filters have higher false track numbers due to the use of the EKF. Also increasing the measurement noise level affects the effective nonlinearity of the estimation problem. Track continuity of the MM-SPHD filter is better than those of the other filters, but the computational complexity of the MM-SPHD filter is slightly higher. In terms of track continuity, MM-SPHD and MM-AP-PHD filters performed nearly the same. As shown in Table III, in terms of OSPA, the MM-SPHD filter performed the best. The OSPA performance can be compared to the PCRLB [2] values.

TABLE III

AVERAGE PERFORMANCE METRICS FROM 1000 MONTE CARLO RUNS ($\sigma_\omega = 2^\circ$, MM-SPHD† - WITH KNOT PREDICTION FROM [24], MM-SPHD‡ - WITH NEW KNOT PREDICTION METHOD)

Filters	OSPA (m)	PCRLB (m)	Number of false tracks	Track continuity (%)	CPU time (sec)
MM-SPHD†	375	295	0.0320	91.65	16.50
MM-SPHD‡	308	295	0.0265	93.05	16.00
MM-GM-USMC-PHD	560	295	0.1325	84.75	9.00
MM-GM-SMC-PHD	685	295	0.1855	78.21	8.55
MM-AP-PHD	472	295	0.0595	89.11	12.55

VII. CONCLUSIONS

In this paper, a Multiple Model Spline Probability Hypothesis Density filter implementation was presented as an alternative implementation to the Sequential Monte Carlo and the Gaussian Mixture MM-PHD filters for maneuvering target tracking problems. The resulting algorithm can handle linear, non-linear, Gaussian, and non-Gaussian models. The MM-SPHD filter can provide continuous estimates of the probability hypothesis density function and it is relatively immune to the degeneracy problem. The MM-SPHD filter can maintain highly accurate tracks by taking advantage of dynamic knot movement, but at the expense of higher computational complexity. The MM-SPHD filter performs well with a few knots and provides continuous state estimates for any system, which leads to non-degenerative results. This new filter, which yields accurate results albeit with a higher computational load, is useful in tracking high-value maneuvering targets (e.g., missiles, submarines, ground targets) in the presence of nonlinearity or non-Gaussianity. However, using the MM-SPHD filter is computationally infeasible in two or three physical dimensions, but alternative method of Spline will be used to solve this complexity problem in the future works.

Algorithm 1 MM-SPHD filter

1) At $(k-1)$, prior SPHD of the dynamic system is available
   · $\mathbf{B}_{k-1|k-1}(\mathbf{x}_{k-1}, \mathbf{M}_{k-1} = \mathfrak{p}) \qquad \mathfrak{p} \in \{1, \ldots, \mathsf{r}\}$
   · Total number of models: r
   · Model index at time $(k-1)$: $\mathbf{M}_{k-1} \in \{1, \ldots, \mathsf{r}\}$
   · Prior knot ($\mathbf{t}_{k-1}$) selection:
      – $\mathbf{t}_{k-1} \in \mathbf{t}^l_{k-1} = \{t^l_{1,k-1}, \ldots, t^l_{\tau,k-1}\}$ where $l = 1, \ldots, n$
      – $\mathbf{t}^l_{k-1} = \begin{cases} t^l_{1,k-1}, \ldots, t^l_{p,k-1} = a \\ t^l_{i+p,k-1} = a + \frac{i(b-a)}{n_s+p-1} \qquad \text{for} \quad i = 1, \ldots, (n_s - p) \\ t^l_{\tau-p,k-1}, \ldots, t^l_{\tau,k-1} = b \end{cases}$
      – Range: $[a, b]$
      – Order: p
      – Input/control points: n_s
      – System dimension: n
      – $\tau = n_s + p$
2) Mixing
   · $\tilde{\mathbf{B}}_{k|k-1}(\mathbf{x}_{k-1}, \mathbf{M}_k = \mathfrak{q}) = \sum_{\mathfrak{p}=1}^{\mathsf{r}} \mathbf{B}_{k-1|k-1}(\mathbf{x}_{k-1}, \mathbf{M}_{k-1} = \mathfrak{p}) \pi_{\mathfrak{p}\mathfrak{q}} \qquad \mathfrak{q} \in \{1, \ldots, \mathsf{r}\}$
   · Initial MM-SPHD matched to multitarget model $\mathfrak{q}$: $\tilde{\mathbf{B}}_{k|k-1}(\mathbf{x}_{k-1}, \mathbf{M}_k = \mathfrak{q})$
   · Markovian model transition probability matrix: $\pi_{\mathfrak{p}\mathfrak{q}}$
   · Prior number of expected targets for the $\mathfrak{q}$-th model: $\hat{N}^{\mathfrak{q}}_{k-1|k-1} = \int_{\mathcal{E}_s} \tilde{\mathbf{B}}_{k|k-1}(\mathbf{x}_{k-1}, \mathbf{M}_k = \mathfrak{q}) d\mathbf{x}_{k-1}$
   · Overall prior number of expected targets: $\hat{N}_{k-1|k-1} = \sum_{\mathfrak{q}=1}^{\mathsf{r}} \hat{N}^{\mathfrak{q}}_{k-1|k-1} \qquad \mathfrak{q} \in \{1, \ldots, \mathsf{r}\}$
2) Prediction
   · $\mathbf{B}_{k|k-1}(\mathbf{x}_k, \mathbf{M}_k = \mathfrak{q}) = \mathbf{B}_{\mathbf{c},k|k-1}(\mathbf{x}_k, \mathbf{M}_k = \mathfrak{q}) \; + \; \mathbf{B}_{\mathbf{s},k|k-1}(X_k, \mathbf{M}_k = \mathfrak{q}) \; + \; \mathbf{B}_{\mathbf{nb},k}(\mathbf{x}_k, \mathbf{M}_k = \mathfrak{q})$
   · MM-SPHD for the existing targets: $\mathbf{B}_{\mathbf{c},k|k-1}(\mathbf{x}_k, \mathbf{M}_k = \mathfrak{q})$
      – Calculate control points: $\mathbb{P}_{j_1,\ldots,j_{2n}}$
      – Predict the knots: $\mathbf{t}_k = \mathbf{t}^1_k, \ldots, \mathbf{t}^n_k$
      – Use (59) to find: $\mathbf{B}_{\mathbf{c},k|k-1}(\mathbf{x}_k, \mathbf{M}_k = \mathfrak{q})$
   · MM-SPHD for the spawned targets: $\mathbf{B}_{\mathbf{s},k|k-1}(X_k, \mathbf{M}_k = \mathfrak{q})$
      – Use same approach as for $\mathbf{B}_{\mathbf{c},k|k-1}(\mathbf{x}_k, \mathbf{M}_k = \mathfrak{q})$
   · MM-SPHD for the newborn targets: $\mathbf{B}_{\mathbf{nb},k}(\mathbf{x}_k, \mathbf{M}_k = \mathfrak{q})$
      – Calculate $P_k(\Im_i, \mathbf{M}_k = \mathfrak{q})$
      – $N_{\mathbf{nb},i} = \begin{cases} 1 \quad \text{if} \;\; P_k(\Im_i, \mathbf{M}_k = \mathfrak{q}) \leqslant \epsilon, \\ 0 \qquad \text{otherwise.} \end{cases}$
      – Use (64) to find $\mathbf{B}_{\mathbf{nb},k}(\mathbf{x}_k, \mathbf{M}_k = \mathfrak{q}) \qquad \mathfrak{q} \in \{1, \ldots, \mathsf{r}\}$
2) Update
   · Updated MM-SPHD: $\mathbf{B}_{k|k}(\mathbf{x}_k, \mathbf{M}_k = \mathfrak{q})$
      – Use (67) to find $\mathbf{B}_{k|k}(\mathbf{x}_k, \mathbf{M}_k = \mathfrak{q})$
      – $\hat{N}^{\mathfrak{q}}_{k|k} = \int_{\mathcal{E}_s} \mathbf{B}_{k|k}(\mathbf{x}_k, \mathbf{M}_k = \mathfrak{q}) d\mathbf{x}_k$
   · Total number of targets:
      – $\hat{N}_{k|k} = \sum_{\mathfrak{q}=1}^{\mathsf{r}} \hat{N}^{\mathfrak{q}}_{k|k} \qquad \mathfrak{q} \in \{1, \ldots, \mathsf{r}\}$
   · Calculate the mode probability

REFERENCES

[1] Bar-Shalom, Y., Willett, P. K., and Tian, X., *Tracking and Data Fusion*, YBS Publishing, Storrs, 2011.

[2] Bar-Shalom, Y., Li, X. R., and Kirubarajan, T., *Estimation with Applications to Tracking and Navigation*, John Wiley, New York, 2001.

[3] Baser, E., and Efe, M., "A novel auxiliary particle PHD filter", *Proceedings of the International Conference on Information Fusion*, pp. 165–172, July 2012.

[4] Buss, R. S., *A Mathematical Introduction with OpenGL*, Cambridge University Press, New York, 2003.

[5] Clark, D., Vo, B.-T., and Vo, B.-N., "Gaussian particle implementations of probability hypothesis density filters", *Proceedings of the IEEE Aerospace Conference*, pp. 1–11, Big Sky, Montana, Mar. 2007.

[6] De Boor, C., *A Practical Guide to Splines*, Springer-Verlag, New York, 2001.

[7] Doucet, A., De Freitas, N., and Gordon, N., *Sequential Monte Carlo Methods in Practice*, Springer, New York, 2001.

[8] El-Fallah, A., Zatezalo, A., Mahler, R. P. S., Mehra, R. K., and Alford, M., "Regularized multitarget particle filter for sensor management", *Proceedings of the SPIE Signal Processing, Sensor Fusion, and Target Recognition XV*, vol. 6235, pp. 1–11, Apr. 2006.

[9] Gorji, A. A., Tharmarasa, R., and Kirubarajan, T., "Performance measures for multiple target tracking problems", *Proceedings of the 14th International Conference on Information Fusion*, pp. 1–8, July 2011.

[10] He, X., Sithiravel, R., Tharmarasa, R., Bhashyam, B., and Kirubarajan, T., "A spline filter for multidimensional nonlinear state estimation", *Signal Processing*, vol. 102, pp. 282–295, Sep. 2014.

[11] Kirubarajan, T., and Bar-Shalom, Y., "Low observable target motion analysis using amplitude information", *IEEE Transactions on Aerospace and Electronic Systems*, vol. 32, no. 4, pp. 1367–1384, Oct 1996.

[12] Li, X. R., and Jilkov, V. P., "Survey of maneuvering target tracking. Part V: Multiple-model methods", *IEEE Transactions on Aerospace and Electronic Systems*,vol. 41, pp. 1255–1321, Oct. 2005.

[13] Mahler, R. P. S., "Multitarget Bayes filtering via first-order multitarget moments", *IEEE Transactions on Aerospace and Electronic Systems*, vol. 39, pp. 1152–1178, Oct. 2003.

[14] Mahler, R. P. S., *Statistical Multisource-Multitarget Information Fusion*, Artech, Norwood, Massachusetts, 2007.

[15] Mahler, R. P. S., "On multitarget jump-Markov filters", *Proceedings of International Conference on Information Fusion*, Singapore, July 2012.

[16] Nardone, S. C., Lindgren, A. G., and Gong, K. F., "Fundamental properties and performance of conventional bearing-only target motion analysis", *IEEE Transactions on Automatic Control*, vol. 29, pp. 775–787, Sep. 1984.

[17] Oudjane, N., and Musso, C., "Progressive correction for regularized particle filters", *Proceedings of International Conference on Information Fusion*, vol. 2, pp. 10–17, Paris, France, July 2000.

[18] Popp, R. L., Kirubarajan, T., and Pattipati, K. R., Chapter 2 *in Multitarget/Multisensor Tracking: Applications and Advances III*, (Bar-Shalom, Y. and Blair, W. D., eds.), Artech House, Norwood, 2000.

[19] Punithakumar, K., McDonald, M., and Kirubarajan, T., "Spline filter for multidimensional nonlinear/non-Gaussian Bayesian tracking", *Proceeding of SPIE*, vol. 6969, pp. 1–8, May. 2008.

[20] Punithakumar, K., Kirubarajan, T., and Sinha, A., "Multiple-model probability hypothesis density filter for tracking maneuvering targets", *IEEE Transactions on Aerospace and Electronic Systems*, vol. 44, pp. 87–98, Jan. 2008.

[21] Petetin, Y., and Desbouvries, F., "A mixed GM/SMC implementation of the probability hypothesis density filter", *Proceedings of the International Conference on Information Science, Signal Processing and Their Applications*, pp. 425–430, July 2012.

[22] Rogers, F. D., *An Introduction to NURBS*, Morgan Kaufmann Publishers, California, 2001.

[23] Sarfraz, M., *Interactive Curve Modeling*, Springer-Verlag, London, 2008.

[24] Sithiravel, R., Chen, X., Tharmarasa, R., Balaji, B., and Kirubarajan, T., "The spline probability hypothesis density filter", *IEEE Transactions on Signal Processing*, vol. 61, no. 24, pp. 6188–6203, Dec. 2013.

[25] Sithiravel, R., Chen, X., McDonald, M., and Kirubarajan, T., "Spline probability hypothesis density filter for nonlinear maneuvering target tracking", *Proceedings of Asilomar Conference on Signals, Systems and Computers*, pp. 1743–1750, Pacific Grove, CA, Nov. 2013.

[26] Schuhmacher, D., Vo, B.-T., and Vo, B.-N., "A consistent metric for performance evaluation of multi-object filters", *IEEE Transactions on Signal Processing*, vol. 56, no. 8, pp. 3447–3457, Aug. 2008.

[27] Straka, O., Dunik, J., and Simandl, M., "Performance evaluation of local state estimation methods in bearings-only tracking problems", *Proceedings of International Conference on Information Fusion*, pp. 1–8, July 2011.

[28] Tang, X., Wei, P., "Multitarget state extraction for the particle probability hypothesis density filter", *IET Radar, Sonar and Navigation*, vol. 5, pp. 877–883, Oct. 2011.

[29] Tobias, M., and Lanterman, A. D., "A probability hypothesis density-based multitarget tracker using multiple bistatic range and velocity measurement", *Proceeding of the Southeastern Symposium on System Theory*, pp. 205–209, Mar. 2004.

[30] Vo, B.-N., Singh, S., and Doucet, A., "Random finite sets and sequential Monte Carlo methods in multi-target tracking", *Proceedings of the international Radar Conference*, pp. 486–491, Sep. 2003.

[31] Vo, B.-N., Singh, S., and Doucet, A., "Sequential Monte Carlo implementation of the PHD filter for multi-target tracking", *Proceedings of International Conference on Information Fusion*, vol. 2, pp. 792–799, July 2003.

[32] Vo, B.-N., and Ma, W.-K., "The Gaussian mixture probability hypothesis density filter", *IEEE Transactions on Signal Processing*, vol. 54, pp. 4091–4104, Nov. 2006.

[33] Whiteley, N., Singh, S., and Godsill, S., "Auxiliary particle implementation of probability hypothesis density filter", *IEEE Transactions on Aerospace and Electronic Systems*, vol. 46, pp. 1437–1454, July 2010.

[34] Yin, J., Zhang, J., and Zhao, J., "The Gaussian particle multi-target multi-Bernoulli filter", *Proceeding of International Conference on Advanced Computer Control*, vol. 4, pp. 556–560, Mar. 2010.

[35] Yoon, J., Kim, D., and Yoon, K., "Gaussian mixture importance sampling function for unscented SMC-PHD filter", *Signal Processing*, pp. 2664–2670, Sep. 2013.

Rajiv Sithiravel received a B.Eng. in Electrical and Computer Engineering from Ryerson University in Toronto, Canada in 2006, M.Eng. degrees in Electrical and Computer Engineering from University of Queensland in Brisbane, Australia in 2007 and from McMaster University in Hamilton, Canada in 2011. PhD degree in Electrical and Computer Engineering from McMaster University, Canada in 2014.

He has been awarded many scholarships including QEII Scholarships in Science and Technology and NSERC's Visiting Fellowship in Canadian Government Laboratories.

From 2008-2009 he was a Consultant in the System Operations Control at Air Canada, Toronto, Canada and he held a post-doctoral position in the Electrical and Computer Engineering department at McMaster University in Hamilton, Canada from 2014 to early 2015. Currently, he has been working as a Defense Scientist in the Radar Sensing and Exploitation division at Department of Research and Development of Canada (DRDC), Ottawa, Canada. At DRDC he has been contributing to numerous airborne sensor based projects including the multisensor data fusion that includes electro-optical (EO) camera, infrared (IR) camera, cardioid sensor, magneto-meter and radar (Synthetic Aperture Radar/Inverse Synthetic Aperture Radar) for Canada's CP-140 program. His research interests include estimation, multitarget tracking, nonlinear filtering, information fusion, signal processing, over the horizon radars, synthetic aperture radar, inverse synthetic aperture radar and magnetic anomaly detection.

Michael McDonald received a B.Sc. (Hons) degree in Applied Geophysics from Queens University in Kingston, Canada in 1986 and a M.Sc. degree in Electrical Engineering in 1990, also from Queen's University. He received a Ph.D. in Physics from the University of Western Ontario in London, Canada in 1997.

He was employed at ComDev in Cambridge, Canada from 1989 through 1992 in their space science and satellite communications departments and contributed to numerous space-based sensor programs including RADARSAT, ERS and NSACT. From 1996 through 1998 he held a post-doctoral position in the Physics department of SUNY at Stony Brooke University undertaking mm-wave spectroscopy of the atmosphere before commencing his current position as a senior Defence Scientist in the Radar Systems and Exploitation (RSE) section of Defence Research and Development Canada (DRDC), Ottawa, Canada. His current research interests include the radar detection and tracking of maritime and land targets, nonlinear filtering for low observable targets, and multisensor fusion for enhanced detection and tracking.

Bhashyam Balaji received his B.Sc. (Hons) degree in physics from St. Stephens College, University of Delhi, India and Ph.D. in theoretical particle physics from Boston University, Boston, MA, in 1997.

Since 1998, he has been a scientist at the Defence Research and Development Canada, Ottawa, Canada. His primary research interests include all aspects of radar sensor outputs, including space-time adaptive processing, multitarget tracking, and meta-level tracking including the application of stochastic context-free grammars to syntactic tracking. His theoretical research also includes the application of Feynman path integral and quantum field theory methods to the problems of nonlinear filtering and stochastic control. His recent research includes theoretical and applied aspects of multisource data fusion, including tracking and fusion of sensor outputs from radar, EO/IR, acoustic, electronic support measures, and magnetic anomaly detection sensors.

Thiagalingam Kirubarajan (S' 95 M' 98 SM' 03) received the B.A. and M.A. degrees in electrical and information engineering from Cambridge University, England, and the M.S. and Ph.D. degrees in electrical engineering from the University of Connecticut, Storrs. Dr Kirubarajan (Kiruba) holds the title of Distinguished Engineering Professor and holds the Canada Research Chair in Information Fusion at McMaster University, Canada. He has published about 350 research articles, 11 book chapters, one standard textbook on target tracking and four edited volumes. He has lead multiple projects on tracking and fusion with support from the Canadian Department of National Defense, US Air Force, US Navy, NASA, NSERC, Ontario Ministry of Research and Innovation, General Dynamics Canada, Raytheon Canada, ComDev/exactEarth, Toyota, Mine Radio Systems, Qualtech, FLIR Radar Systems and Lockheed Martin Canada. As part of his research at McMaster University, Dr Kirubarajan led the design and development of the distributed multisensor-multitarget tracking testbed for scenario generation, tracking algorithm development and performance evaluation. In addition to conducting research, he has worked extensively with government labs and companies to process real data and to transition his research to the real world. Through his company TrackGen (www.trackgen.com), he has developed a number of software programs, including MultiTrack for real-time large-scale multisensor-multitarget tracking, MultiFuse for distributed tracking, SceneGen for surveillance scenario simulation, and ISR360 for visualization, performance analysis and situation awareness, which have been integrated into many fielded systems. He is a recipient of Ontario Premiers Research Excellence Award and IEEE AESS Barry Carlton Award.